RESEARCH ARTICLE

Infection-generated electric field in gut epithelium drives bidirectional migration of macrophages

Yaohui Sun[1,2]*, Brian Reid[1], Fernando Ferreira[1,3], Guillaume Luxardi[1], Li Ma[1,4], Kristen L. Lokken[5], Kan Zhu[1]¤, Gege Xu[6], Yuxin Sun[1]¤, Volodymyr Ryzhuk[1], Betty P. Guo[7], Carlito B. Lebrilla[6], Emanual Maverakis[1], Alex Mogilner[2]*, Min Zhao[1]*

1 Department of Dermatology, School of Medicine, University of California, Davis, Sacramento, California, United States of America, **2** Courant Institute and Department of Biology, New York University, New York, New York, United States of America, **3** Departamento de Biologia, Centro de Biologia Molecular e Ambiental (CBMA), Universidade do Minho, Braga, Portugal, **4** Skin and Cosmetic Research Department, Shanghai Skin Disease Hospital, Shanghai, China, **5** Department of Microbiology and Immunology, School of Medicine, University of California, Davis, Davis, California, United States of America, **6** Department of Chemistry, University of California, Davis, Davis, California, United States of America, **7** Office of Research, School of Medicine, University of California, Davis, Davis, California, United States of America

¤ Current address: Department of Radiology and Biomedical Imaging, University of California, San Francisco, San Francisco, California, United States of America
* yhsun@ucdavis.edu (YS); mogilner@cims.nyu.edu (AM); minzhao@ucdavis.edu (MZ)

Abstract

Many bacterial pathogens hijack macrophages to egress from the port of entry to the lymphatic drainage and/or bloodstream, causing dissemination of life-threatening infections. However, the underlying mechanisms are not well understood. Here, we report that *Salmonella* infection generates directional electric fields (EFs) in the follicle-associated epithelium of mouse cecum. In vitro application of an EF, mimicking the infection-generated electric field (IGEF), induces directional migration of primary mouse macrophages to the anode, which is reversed to the cathode upon *Salmonella* infection. This infection-dependent directional switch is independent of the *Salmonella* pathogenicity island 1 (SPI-1) type III secretion system. The switch is accompanied by a reduction of sialic acids on glycosylated surface components during phagocytosis of bacteria, which is absent in macrophages challenged by microspheres. Moreover, enzymatic cleavage of terminally exposed sialic acids reduces macrophage surface negativity and severely impairs directional migration of macrophages in response to an EF. Based on these findings, we propose that macrophages are attracted to the site of infection by a combination of chemotaxis and galvanotaxis; after phagocytosis of bacteria, surface electrical properties of the macrophage change, and galvanotaxis directs the cells away from the site of infection.

Author summary

Bacterial pathogens can invade and survive within macrophages and use them as a vehicle to reach important organs of a human body, resulting in life-threatening infections, but

the underlying mechanisms are not well understood. Our current understanding is that macrophages are recruited to the infected site by sensing gradients of chemokines and/or cytokines released by damaged cells—a process known as chemotaxis. However, this mechanism does not explain how macrophages containing the pathogens escape the site to reach the bloodstream. Here, we use a disseminated *Salmonella* infection model in mice and detect electric fields (EFs) generated by *Salmonella* infection at the gut epithelium, which can drive unidirectional migration of macrophages towards the anode—a biological process also known as galvanotaxis. We further demonstrate that macrophage galvanotaxis can be reversed to the cathode by phagocytosis of the bacteria. Based on these findings, we propose that macrophages are attracted to the site of infection by a combination of chemotaxis and galvanotaxis; after phagocytosis of bacteria, the electrical properties of the macrophage change, and galvanotaxis directs the cells away from the site of infection allowing the escape of the macrophages that contain pathogens.

Introduction

Common bacterial pathogens such as *Salmonella*, *Shigella*, and *Yersinia* spp. invade the gut epithelial barrier, preferentially by targeting the relatively small number of M cells located in the follicle-associated epithelium (FAE) [1–3]. Disruption of epithelial integrity releases chemokines that attract immune cells such as neutrophils and macrophages—a process known as chemotaxis [4–7]. Subsequent phagocytosis and clearance of these pathogens by immune cells usually stops the infection. However, some of these bacterial pathogens have developed strategies, such as the type III secretion systems in *Salmonella* spp. [8–12], to evade macrophage killing and survive inside the macrophage [13–16], an environment in which the pathogen is hidden from the immune system. Survival within the macrophage allows the pathogen to spread from its entry site to the spleen, liver, bone marrow, and other organs via the bloodstream, resulting in life-threatening consequences [17–19]. Although chemotaxis can explain how macrophages reach an infected site, it cannot explain how macrophages harboring pathogens escape from the bacterial entry site to reach the lymphatic drainage and/or bloodstream, a critical initial step in the dissemination process that is understudied and poorly understood.

Bioelectric signals have been implicated in development [20–23], wound healing [24–26], and regeneration [27,28]. For example, a wound collapses the transepithelial potential (TEP) difference of an intact epithelial barrier, generating laterally oriented endogenous electric fields (EFs) of up to 1.4 V cm^{-1}, as well as local electric current densities (J_I) of several μA cm^{-2}. These bioelectric phenomena actively control wound healing in the skin and cornea [25,29]; however, they are extremely challenging to study in the gut epithelium due to limited accessibility and have never been characterized in vivo during an active infection. Nonetheless, it is generally appreciated that an EF on this scale can drive directional cell migration—a process known as electrotaxis or galvanotaxis [21]. Many cell types, regardless of their origin, respond to an exogenous EF by directional migration toward the cathode [25,30], whereas others, e.g., human keratinocytes (HaCat cells) and bone marrow mesenchymal stem cells, migrate toward the anode [31]. Macrophages and lymphocytes also undergo galvanotaxis in vitro and in vivo [32–34].

In the present study, we have developed an ex vivo mouse cecum model of *Salmonella* infection that enables bioelectricity measurement. We report that *Salmonella* infection generates a directional EF at the bacterial entry sites that can recruit macrophages by galvanotaxis. We demonstrate that primary macrophages reverse galvanotaxis direction upon *Salmonella*

infection by modifying their surface glycan composition, which reduces the negative electric charge on the surface. This directional switch is independent of the *Salmonella* pathogenicity island 1 (SPI-1) type III secretion system, a major virulence determinant responsible for *Salmonella* invasion. Instead, it may require certain glycosidases that are widely conserved in *Salmonella* spp., because cleavage of surface-exposed sialic acids with a potent neuraminidase caused severe defects of macrophage galvanotaxis.

Results and discussion

Development of an ex vivo mouse cecum model of *Salmonella* infection for bioelectric characterization

The mouse is an ideal organism for understanding human infectious diseases and is widely used to study bacterial pathogenesis and mucosal immunity of enteropathogenic bacteria [35–40]. Previously, we have successfully measured bioelectric currents in various tissue and organ cultures using the noninvasive vibrating probe [41–44]; however, measuring bioelectric currents in the mouse small intestinal epithelium is challenging due to limited accessibility [45]. Therefore, we developed a new ex vivo cecum model for measuring bioelectric activity in the gut epithelium (S1 Fig). This model is based on the well-established mouse typhoid model, in which mice orally infected with *Salmonella enterica* serotype Typhimurium (*S.* Typhimurium) develop disseminated infection that mimics human typhoid disease [36]. Although the ileum is the most commonly targeted organ to study pathogen–host interactions in vivo, it is too small for the bioelectrical measurements in our ex vivo experimental setting. Instead, the size of the mouse cecum is anatomically optimal. *Salmonella* invades the cecum in mice and causes acute appendicitis in humans [46]. Furthermore, we can easily identify the FAE under a dissecting microscope, because we found that 90% of C57BL/6 mice have only 1 Peyer's patch around the blind-end apex, containing 6 to 11 lymphatic follicles.

Active bioelectricity pervades the FAE in the healthy murine cecum

Using microelectrodes [28] in the ex vivo mouse cecum model, we measured a TEP of up to 15 mV, lumen-positive in uninfected mice. Notably, the TEP in the FAE was significantly smaller than that of the surrounding villi (Fig 1A). Next, using a vibrating probe to measure the J_I close to the gut surface, we detected outward currents at the FAE and inward currents at the villus epithelium, with a magnitude of around 1 μA cm^{-2} (Fig 1B). Such currents were not detected in the serosal epithelium, despite the presence of a TEP (Fig 1A), nor in formalin-fixed epithelia (Fig 1B), suggesting the existence of active bioelectricity restricted to the mucosal epithelium.

It has been well appreciated that mammalian intestinal mucosa maintains a large transmucosal potential difference [47,48]. In humans, that potential is up to 12 mV, lumen-negative, in the fasting jejunum and ileum [49,50]. Rats, mice, chickens, and fish all maintain a TEP of up to 5 mV in their intestinal epithelium, as measured with Ussing chambers [51–55]; however, these measurements provide no spatiotemporal information [45]. The TEP of control murine ceca (up to 15 mV) that we have measured directly with glass electrodes under microscopic resolution were well within the physiological range described above; however, it differed spatially, i.e., the TEP of the FAE was significantly lower than the TEP of the surrounding villus epithelium (Fig 1A). Using an ultrasensitive vibrating probe, we further detected ionic currents that run in opposite directions between the FAE and surrounding villi (Fig 1B). Together, these findings unveil lateral voltage gradients and/or constant current loops running between these two structurally and functionally distinct epithelia. In the normal gut scenario, such a
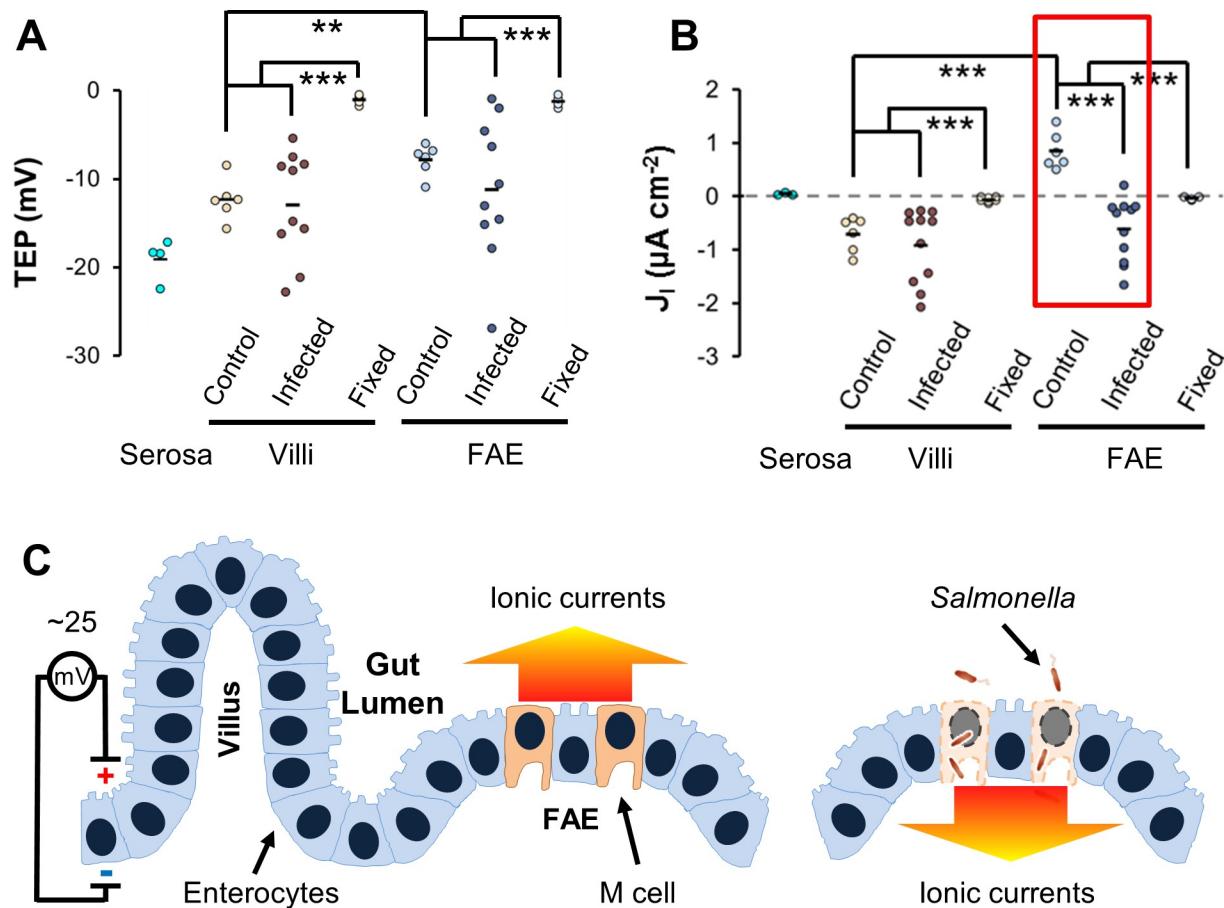
Fig 1. IGEF at gut epithelium. (A) TEP and (B) Peak ionic current density (J_I) in mock-infected mice ("Control") or *Salmonella*-infected mice ("Infected") at 16 to 40 h PI. Each dot represents an average of 3 to 5 FAEs or villus epithelium ("Villi") of each mouse. Serosal epithelia ("Serosa") and formalin-fixed mouse ceca ("Fixed") served as controls. ∗∗$P < 0.01$, ∗∗∗$P < 0.001$ by one-way ANOVA with post hoc Tukey HSD test (see S1 Data). The red box highlights *Salmonella* infection-generated current reversal at the FAE. (C) The diagram depicts an IGEF generated by *Salmonella* infection at the gut epithelium in a mouse model of human typhoid fever. TEP of up to 25 mV, lumen-positive, occurs across a single layer of tightly sealed gut epithelium and drives micro-ionic currents running from the epithelial surface to the lumen (color-coded arrow indicates the direction of current flow). *Salmonella* invades and breaks epithelial integrity, preferentially at the FAE, which reverses ionic currents running from the breached epithelium into the deep intestinal wall (color-coded arrow indicates the direction of current flow). FAE, follicle-associated epithelium; HSD, honest significant difference; IGEF, infection-generated electric field; PI, post infection; TEP, transepithelial potential.

https://doi.org/10.1371/journal.pbio.3000044.g001

bioelectrical landscape may prevent commensals from accidentally entering the FAE and enable the pathogens to specifically target M cells via bacterial galvanotaxis [56].

Salmonella infection generates bioelectric fields at the FAE of its entry site

Salmonella invades the intestinal epithelium, preferentially by targeting M cells located at an FAE [1,57]. If a wound disrupting an epithelium can generate a steady EF, one would envisage that similar EFs must be produced at the *Salmonella* entry site because of the breakage of epithelial integrity and subsequent short-circuit of the transmucosal potential difference. This is indeed the case in our model. In mice intragastrically challenged with *S.* Typhimurium, the peak J_I remarkably reversed to become inward in FAE compared to control mice, whereas that of the villus epithelium increased nonsignificantly (Fig 1B). Consistent with this finding, we also detected high variation in TEP from individual *S.* Typhimurium–infected mice (up to 25

mV), still lumen-positive (Fig 1A), which has also been observed in chemically induced colitis in rats [58]. More importantly, penetrating electrodes through disrupted FAE up to 200 μm in depth revealed a stepwise increase in TEP (S2 Fig), suggesting the existence of an electric potential gradient generated by the *S*. Typhimurium infection.

Bacterial invasion and subsequent dissemination to mesenteric lymph nodes (MLNs) and spleen were verified by determination of colony-forming units (CFUs) (S4A Fig), and disruption of FAE was assessed by histological staining (S4B Fig). *S*. Typhimurium was undetectable in some of the MLNs and spleens, indicating that some of the FAE and surrounding villi were either uninfected or mildly infected, which explains the wide distribution of TEP and J_I measured in the *S*. Typhimurium–challenged mice.

Based on these results, we coined the term infection-generated electric field (IGEF) (Fig 1C) to distinguish it from a wound-generated electric field (WGEF) [26]. We demonstrate, for the first time, that *Salmonella* infection generated a steady EF (up to 5 V cm^{-1}, provided an epithelial thickness of 50 μm) that drives minute directional electric currents, running from the breached FAE into the deep intestinal wall in a stepwise manner. Although how the IGEFs are formed is currently unknown, we speculate on a couple of possible mechanisms. First, in order to establish a steady EF, a potential gradient or a circuit must be formed. Even though there are accumulated charges segregated by the epithelium (positive at the apical side), in a healthy gut a circuit is unlikely to be formed by the epithelium itself due to high resistance of the epithelium, which is sealed by tight junctions. However, given that the intestinal lumen is alkaline (more negative in terms of electrogenesis), a micropotential gradient could be developed in close proximity to the apical side of the gut epithelia, which can drive outward ionic currents (Fig 1C). Second, differential expression and asymmetric distribution of ion pumps and channels essential for selective absorption and/or secretion of electrogenic ions by enterocytes and M cells [47,48] are likely to be critical for the generation of the aforementioned bioelectricity. Future studies using specific channel blockers in combination with our bioelectrical experimental model and techniques will help to pinpoint the molecular mechanism of an IGEF by identifying the channel(s) or pump(s) involved. Third, as in the formation of a WGEF [21,59], *Salmonella* preferentially invades and destroys M cells and collapses the epithelial barrier at the FAE (S4B Fig), which short-circuits the TEP. Subsequently, the short-circuited and augmented TEP could then drive inward ionic currents as supported by the measurements of stepwise increase of the TEP (S2B Fig). Fourth, in contrast to the healthy alkaline gut, the microenvironment at the *Salmonella* entry site (i.e., the FAE) is likely to be more acidic (more positive in terms of electrogenesis) because of the local inflammatory responses [60] and metabolic changes [61] induced by *Salmonella* infection. Such a microenvironmental pH switch could be related or attributed to the reversal of ionic current flow as we detected with vibrating probes (Fig 1B). Like the injury currents reported by Sawyer and colleagues in early publications [62–64], IGEF-driving ionic currents could affect small blood vessels in the intestinal wall and mesentery to cause a transvascular potential drop or reversal, resulting in 2 possible consequences: an intravascular occlusion that may benefit transendothelial penetration of immune cells (e.g., monocytes, leukocytes) and/or the creation of a galvanotactic route between the infected epithelium and the electrically impacted vessels [65].

Salmonella reverses the directional migration of IGEF-guided macrophage galvanotaxis in vitro

Although IGEFs may provide a guidance cue for the enterocytes or even local stem cells, contributing to the repair process of damaged epithelium, the major focus of this work is, rather, to investigate its biopathological role in the systemic *Salmonella* infection, specifically during

the initiation of macrophage-driven dissemination. Previous studies have shown that applying an EF in vitro can direct macrophage galvanotaxis to the anode [32–34]. We confirmed this phenotype by demonstrating that the primary mouse peritoneal macrophages (PMs), in response to an exogenous EF tuned to mimic the in vivo IGEF (mathematics in Materials and methods), underwent robust unidirectional migration to the anode (S1 Movie). This unidirectional migration was verified by immunostaining showing that nearly 100% of macrophages were polarized to the anode with a distinct morphology characterized by a leading pseudopodium of dense actin meshwork and a rearward uropod. However, upon challenge with *S.* Typhimurium IR715, the average directionality of EF-induced galvanotaxis decreased significantly, with approximately 41% of the macrophages reversing their migratory direction from the anode to the cathode (Fig 2 and S2 Movie). Although PMs have been widely used in bacterial infection studies [66], likely due to the ease of harvesting, the most commonly used primary murine macrophages are the bone marrow-derived macrophages (BMDMs) because of their high yield and less heterogeneous nature, which makes them phenotypically and functionally different from PMs [67]. To exclude the possibility that the observed bidirectional migration is restricted to PMs, we generated and tested galvanotaxis of BMDMs as we did with PMs. Although both types of macrophages exhibited similar unidirectional migration (mean directionality: −0.98 versus −0.88) to the anode, reversal in BMDMs infected by *Salmonella* IR715 was more robust than in PMs infected by the same *Salmonella* strain (mean directionality: 0.36 versus −0.18) (Fig 2C and S5B Fig). Notably, this phenotype can be reproduced in BMDMs challenged by another 2 virulent *S.* Typhimurium strains, LT2 and SL1344 (S5 Fig), suggesting that directional migration in response to electrical stimuli is an intrinsic hallmark of the macrophages regardless of their origins and that the ability to manipulate and subvert galvanotaxis in these macrophages is conserved in virulent *Salmonella* spp.

If the cells had simply stopped sensing the EF, then we would have observed random migration, as was the case for control macrophages not subjected to an EF (Fig 2E). The observed change in migration pattern can be attributed to *S.* Typhimurium infection for a variety of reasons. First, a gentamycin protection assay confirmed the presence of intracellular bacteria (Fig 2D); second, flow cytometry demonstrated a high *S.* Typhimurium infection rate (approximately 53%) (S6 Fig); and third, high-resolution confocal microscopy revealed that macrophages containing intracellular *S.* Typhimurium switched polarity to the cathode (Fig 2G). Based on these findings, we conclude that *Salmonella*-containing macrophages respond to galvanotaxis stimuli by reversing their primary directional migration.

Infection-dependent directional switch of macrophage galvanotaxis is SPI-1 independent

Macrophages are professional phagocytes that uptake a broad range of substances; meanwhile, pathogenic *Salmonella* has developed several virulence means to evade macrophage killing, with SPI-1 being the major virulence factor responsible for colonization and invasion [10,68]. To better understand whether the directional reversal is phagocytosis dependent or SPI-1 specific, we monitored galvanotaxis under identical conditions in BMDMs challenged with (i) fluorescently labeled microspheres similar in size to bacteria, (ii) *S.* Typhimurium constitutively expressing mCherry, and (iii) a green fluorescent protein (GFP)-expressing Δ*invA* mutant that lacks a functional SPI-1 (unable to inject its effectors into cells) [69] (Fig 3A). Macrophages challenged with microspheres exhibited migratory behavior similar to that of controls, i.e., unidirectional migration to the anode (Fig 3B and S3 Movie). Macrophages challenged with Δ*invA* migrated with a significantly decreased overall directionality close to that of macrophages infected with wild-type (WT) *Salmonella* (Fig 3B), even though the number of
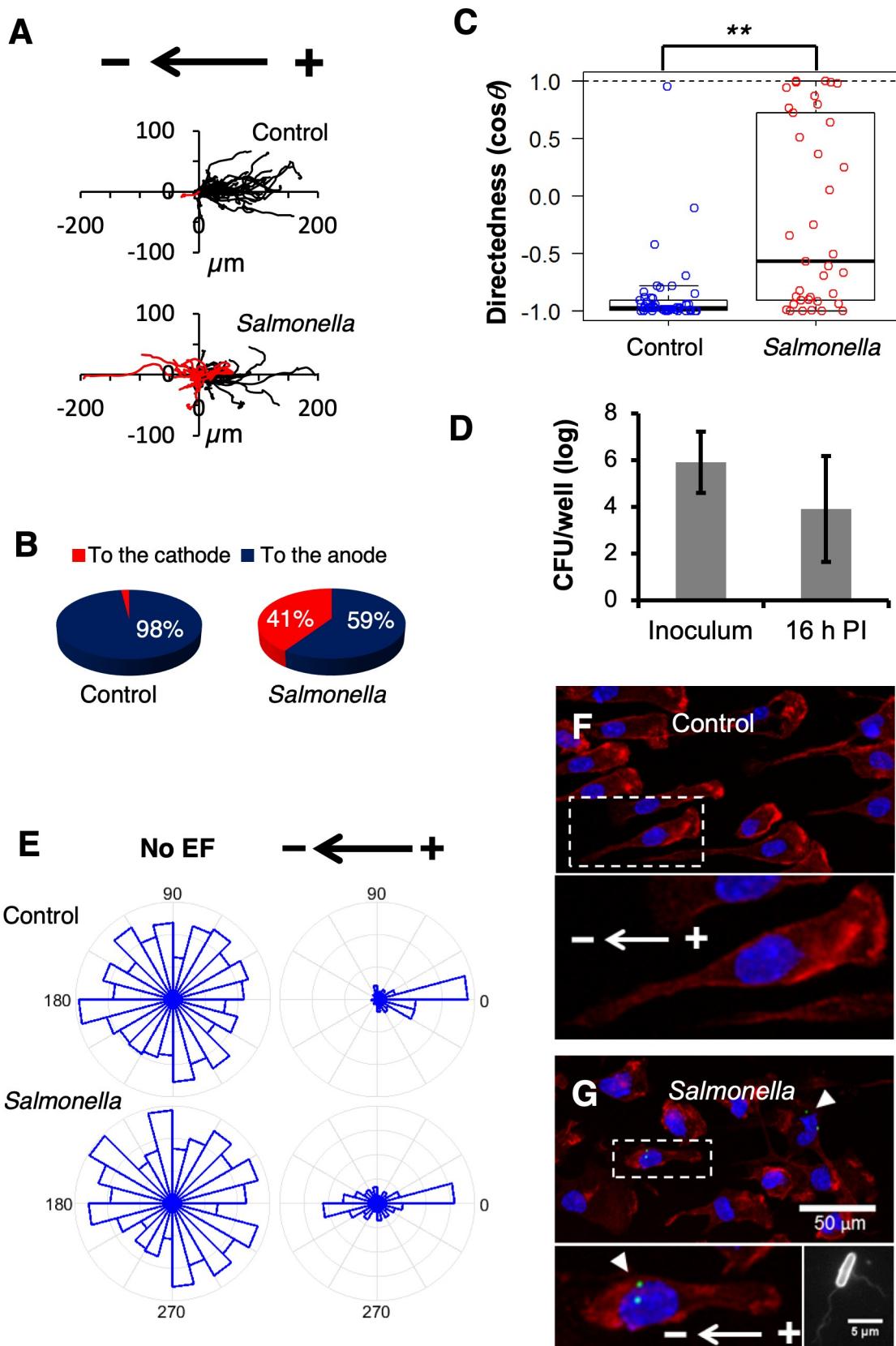
Fig 2. *Salmonella* infection switches macrophage galvanotaxis to the cathode. (A) Trajectories of PMs exposed to an IGEF-mimetic EF of 4 V cm^{-1} for 3 h in the indicated orientation before or at 16 h PI. Each line represents one cell's trajectory. (B) Pie charts show percentage of cells migrating to the cathode (red) or to the anode (blue) as demonstrated in panel A. (C) Quantification of overall directionality as directedness. Directedness is calculated as cosθ, in which θ is the angle of each cell traveled corresponding to the applied EF field (positive, to the cathode; negative, to the anode). Data from a representative of multiple independent experiments are represented by jitter plots with boxes indicating the median, the quartile 1/quartile 3, and the minimum/maximum. $^{**}P < 0.01$ by unpaired Student t test (see S1 Data). (D) Intracellular bacteria were quantified per gentamycin protection assay in 24-well plates and normalized by inoculum. Data from triplicate wells are presented as mean ± SE. (E) Rose plots show random migration of PMs with no EF, unidirectional migration (to the anode) of control macrophages in response to an EF of 4 V cm^{-1}, and bidirectional migration (either to the anode or the cathode) of cells infected with *Salmonella* exposed to the same EF (see S1 Data). (F) A representative confocal image shows that control PMs were polarized to the anode with a characteristic morphology: massive actin meshwork labeled by Alexa Fluor 555 Phalloidin (red) in the front and a uropod at the rear. Nuclei were labeled by Hoechst 33342 (blue). Bottom panel shows enlargement of the checked area in the indicated field. (G) A representative confocal image showing that macrophages with intracellular *Salmonella* (white arrowheads) were polarized to the cathode. Intracellular *Salmonella* were detected by a specific antibody that recognizes both cell body and flagellae (bottom right panel) and stained with a secondary antibody conjugated with Alexa Fluor 488 (green). Actin and nuclei were stained as in panel F. Bar, 50 μm. Bottom left panel shows enlargement of the checked area in the indicated field. CFU, colony-forming unit; EF, electric field; IGEF, infection-generated electric field; PI, postinfection; PM, peritoneal macrophage; SE, standard error; cosθ, cosine theta.

https://doi.org/10.1371/journal.pbio.3000044.g002

intracellular mutants was indeed lower than that of the WT (Fig 3C). Time-lapse recording captured a marked opposing directional migration pattern: macrophages containing microspheres migrated to the anode, and macrophages with either WT or Δ*invA* bacteria inside migrated to the cathode (Fig 3D and 3E, and S3 Movie), further confirming that the observed directional switch was *Salmonella* infection dependent. There were similar phagocytosis and/or infection rates between the macrophages challenged with microspheres or *Salmonella* in the given multiplicity of infection (MOI; S7A and S7B Fig), as verified by flow cytometry (S6 Fig). Cells containing no or variable microspheres migrated to the anode exclusively (S7C and S7D Fig), ruling out mechanisms solely based on phagocytosis. The fact that cells containing either WT or Δ*invA* migrated to the cathode suggests that the SPI-1 type III secretion system is not required or, at least, is insufficient for the directional switch. These data are in accordance with previous studies that identified an SPI-1-independent pathway contributing to early dissemination of *S.* Typhimurium in the mouse typhoid model [17]. We therefore argue for the existence of a general infection-dependent mechanism that involves phagocytosis and subsequent interplay between the macrophages and internalized bacterial pathogens.

Salmonella but not microspheres decreases surface-exposed sialic acids in macrophages

Charged cell-surface components are critical for EF-induced motility in 3H3 cells [70] and have been implicated in electro-osmosis of concanavalin A (Con A) binding receptors on the surface of myotomal spheres [71]. We hypothesized that the directional switch of macrophage galvanotaxis could result from bacteria-induced modifications to the charged components of the cell surface, which would not occur following microsphere challenge (Fig 4A). To this end, we screened *Salmonella*-infected and control macrophages against a panel of fluorescently labeled lectins (glycan-binding proteins) capable of detecting charged and uncharged cell surface glycans (S1 Table). The normalized mean fluorescent intensity of Maackia Amurensis Lectin II (MAL-2), a lectin that recognizes pathogen-binding sialic acids, was significantly decreased in macrophages infected by *Salmonella* but not in those carrying microspheres (Fig 4B–4D). Marked Galanthus Nivalis Lectin (GNL)- and Con A–binding aggregates were visible within macrophages infected by *Salmonella* (S8 and S9 Figs), raising the possibility that the decrease in MAL-2-binding sialic acids could be the result of bacterial internalization and subsequent degradation.
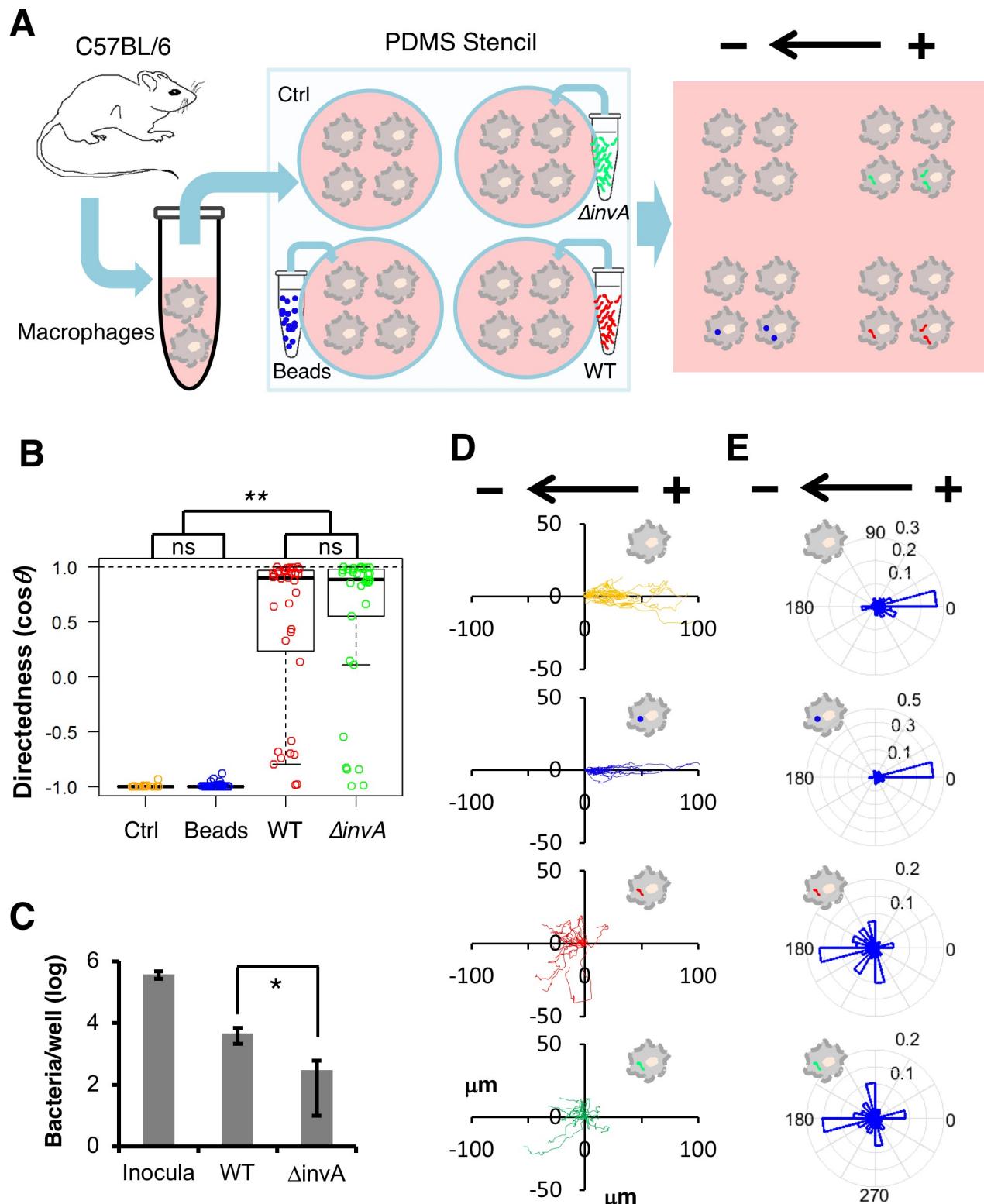
Fig 3. Directional switch mediated by *Salmonella* infection in macrophage galvanotaxis is phagocytosis independent and SPI-1 independent.
(A) Schematic of the experimental design. Freshly differentiated mouse BMDMs were seeded in wells engineered with a PDMS stencil. Adhered macrophages were challenged with either blue fluorescent beads ("Beads") or WT *Salmonella* expressing mCherry (WT) or SPI-1 mutants expressing GFP (*ΔinvA*) and cultured for 16 h. Unchallenged BMDMs served as the Ctrl. Subsequent migration of macrophages was monitored in the same galvanotaxis chamber under identical conditions after removal of the PDMS stencil. (B) Directedness of macrophages under different challenge

conditions. $^{**}P < 0.01$ by one-way ANOVA with post hoc Tukey HSD test (see S1 Data). (C) Intracellular bacteria were quantified per gentamycin protection assay in 24-well plates and normalized by inoculum. Data from triplicate wells are presented as mean ± SE. $^{*}P < 0.05$ by unpaired Student t test. (D) Trajectories of Ctrl macrophages (orange) or macrophages bearing beads (blue) or WT (red) or Δ$invA$ (green) exposed to an EF of 4 V cm^{-1} for 3 h in the indicated orientation. (E) Rose plots show opposite galvanotactic behaviors of Ctrl macrophages or macrophages bearing beads (to the anode) or macrophages containing WT or Δ$invA$ (to the cathode) (see S1 Data). See also S3 Movie. BMDM, bone marrow-derived macrophage; Ctrl, control; EF, electric field; GFP, green fluorescent protein; HSD, honest significant difference; ns, nonsignificant; PDMS, polydimethylsiloxane; SE, standard error; SPI-1, *Salmonella* pathogenicity island 1; WT, wild type.

https://doi.org/10.1371/journal.pbio.3000044.g003

Cleavage of surface-exposed sialic acids impairs macrophage galvanotaxis via zeta potential

Sialylated cell surface molecules are negatively charged, creating an electronegative zeta potential [72]. Using an electrophoretic light-scattering technique, we determined the zeta potential
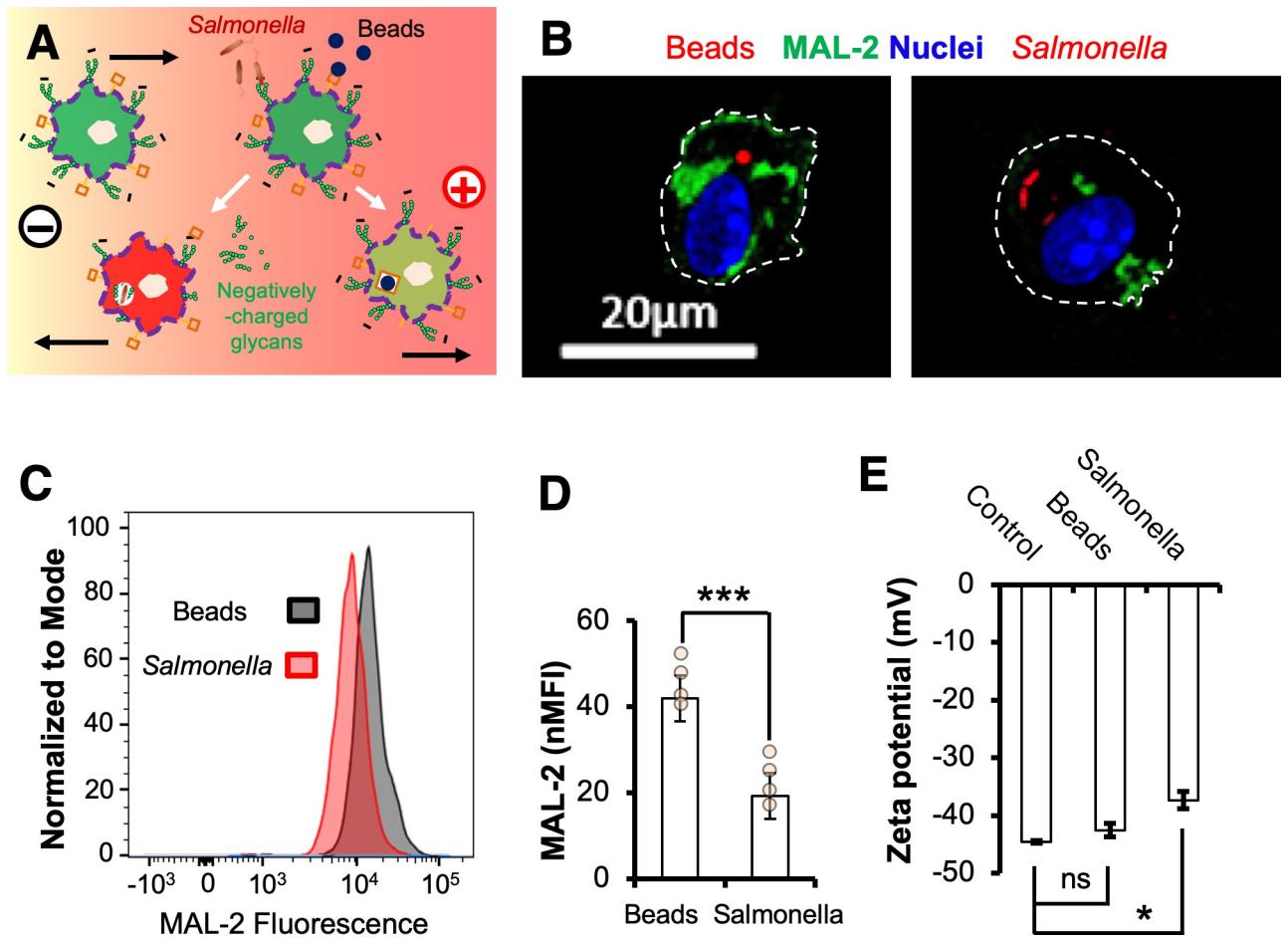

Fig 4. *Salmonella* infection but not challenge by microspheres decreases surface-exposed sialic acids and reduces the negativity of BMDMs. (A) Schematic showing the simplified hypothesis of galvanotaxis in macrophages and a directional switch modulated by *Salmonella* infection. Primary macrophages with sialylated glycoproteins or lipids (small green circles) migrate to the anode. Activated macrophages with reduced negativity, either through enzymatic activities of the *Salmonella* or internalization and/or degradation, switch direction to the cathode, whereas macrophages that phagocytosed beads via nonsialylated surface components (brown squares) still migrate to the anode. (B) Representative confocal images of surface MAL-2 (green) of BMDMs challenged with 1-μm diameter red fluorescent microspheres or *S*. Typhimurium constitutively expressing mCherry (red) at 16 h PI. Nuclei were counterstained with DAPI (blue). Bar, 20 μm. (C) Representative flow cytograms and (D) independent data of standardized MAL-2 fluorescence (green) intensity of BMDMs treated as in panel B. $^{***}P < 0.001$ by Student t test. (E) Zeta potential of control BMDMs or BMDMs challenged with beads or *S*. Typhimurium at 16 h PI. Data quantified from a representative of 3 independent experiments are presented as mean ± SE. $^{*}P < 0.05$ by one-way ANOVA with post hoc Tukey HSD test (see S1 Data). BMDM, bone marrow-derived macrophage; HSD, honest significant difference; MAL-2, Maackia Amurensis lectin II; ns, nonsignificant; PI, post infection; SE, standard error; *S*. Typhimurium, *Salmonella enterica* serotype Typhimurium.

https://doi.org/10.1371/journal.pbio.3000044.g004

of BMDMs under various conditions. The negative zeta potential of macrophages infected by *S*. Typhimurium was significantly reduced, i.e., less negative than that of control macrophages ($P < 0.05$) (Fig 4E). By contrast, macrophages challenged with microspheres showed a nonsignificant zeta potential change compared to that of control macrophages (Fig 4E), suggesting that the decrease in surface-exposed sialic acids and subsequent reduction of surface negativity is mediated by active bacterial product(s) [73].

If a decrease of the negatively charged sialic acids of the surface glycoproteins is critical for the directional switch in macrophage galvanotaxis, then cells with their sialic acids enzymatically removed should exhibit a switch or at least a defect in directional migration when exposed to an EF. To test this, we treated freshly isolated mouse BMDMs with a potent neuraminidase (an enzyme that cleaves terminal sialic acid residues from surface-exposed glycoproteins) [74]. Cleavage of sialic acids following enzymatic treatment was confirmed by flow cytometry and confocal microscopy (Fig 5A–5C). As predicted, the zeta potentials of neuraminidase-treated macrophages were significantly reduced (Fig 5D). These cells also lost anodal migration compared to control macrophages monitored in parallel (Fig 5E and 5F, and S4 Movie). Further inspection and morphological quantification of macrophages stained with fluorescently labeled actin and/or lectin revealed that 71% of the macrophages treated with neuraminidase failed to establish a polarity and notably, 12% of the cells were polarized to the cathode whereas nearly all the control macrophages (97%) were polarized to the anode in response to the EF (Fig 5G).

It is well known that a change in the environmental pH can dramatically influence the growth and virulence of *Salmonella* [75,76]. Moreover, by exposure to acidic pH, a condition that is required for activation of several *Salmonella* virulence factors [77–79], it is possible to modify macrophage surface electrical properties [30]. Therefore, to further determine the importance of surface negativity, we incubated BMDMs in medium at pH 5.8 that markedly reduced the zeta potential (S11A Fig), presumably through protonation of the sialylated surface molecules. Similar to the neuraminidase treatment, galvanotaxis of BMDMs under acidic conditions was significantly impaired, resulting in nearly half of the macrophages (47%) losing their directional migration and 14% of the macrophages reversing their polarity to the cathode (S11B-S11D Fig and S5 Movie). Although these data are consistent with our previous studies, showing that low pH abrogates directional migration of epithelial cells in response to an EF [80,81], it also suggests that the acidic environment is not only required for the activation of *Salmonella* but also contributes to triggering dissemination.

How does *Salmonella* infection instruct macrophages to reverse EF-directed migration? Firstly, it is important to note that infecting macrophages with a SPI-1 mutant resulted in a directional switch similar to that of WT, with nearly all the macrophages containing live fluorescent protein-expressing bacteria migrating to the cathode (Fig 3 and S3 Movie). This suggests a general mechanism, independent of this major virulence factor, even though other specific factor(s) may still be involved [82,83]. Previously reported effects have suggested that negatively charged surface glycan moieties are critical for EF-induced cell motility and polarization, which are consistent with our data, and provide a long sought-after mechanism of action. Because macrophages challenged with microspheres did not show a significantly reduced zeta potential (Fig 4E), it is likely that the decrease in surface-exposed sialic acids and reduction of surface negativity is mediated by active bacterial product(s) rather than by metabolic changes in the host itself. It is also important to note that although both *Salmonella* infection and neuraminidase treatment decreased the surface-exposed sialic acids, the latter caused a serious defect in macrophage galvanotaxis without reversing the overall directionality (Fig 5E), in contrast to *Salmonella* infection (Fig 3B). There may be multiple glycosidases involved in surface glycan modification to reverse directionality (Fig 5H) because *Salmonella* possesses
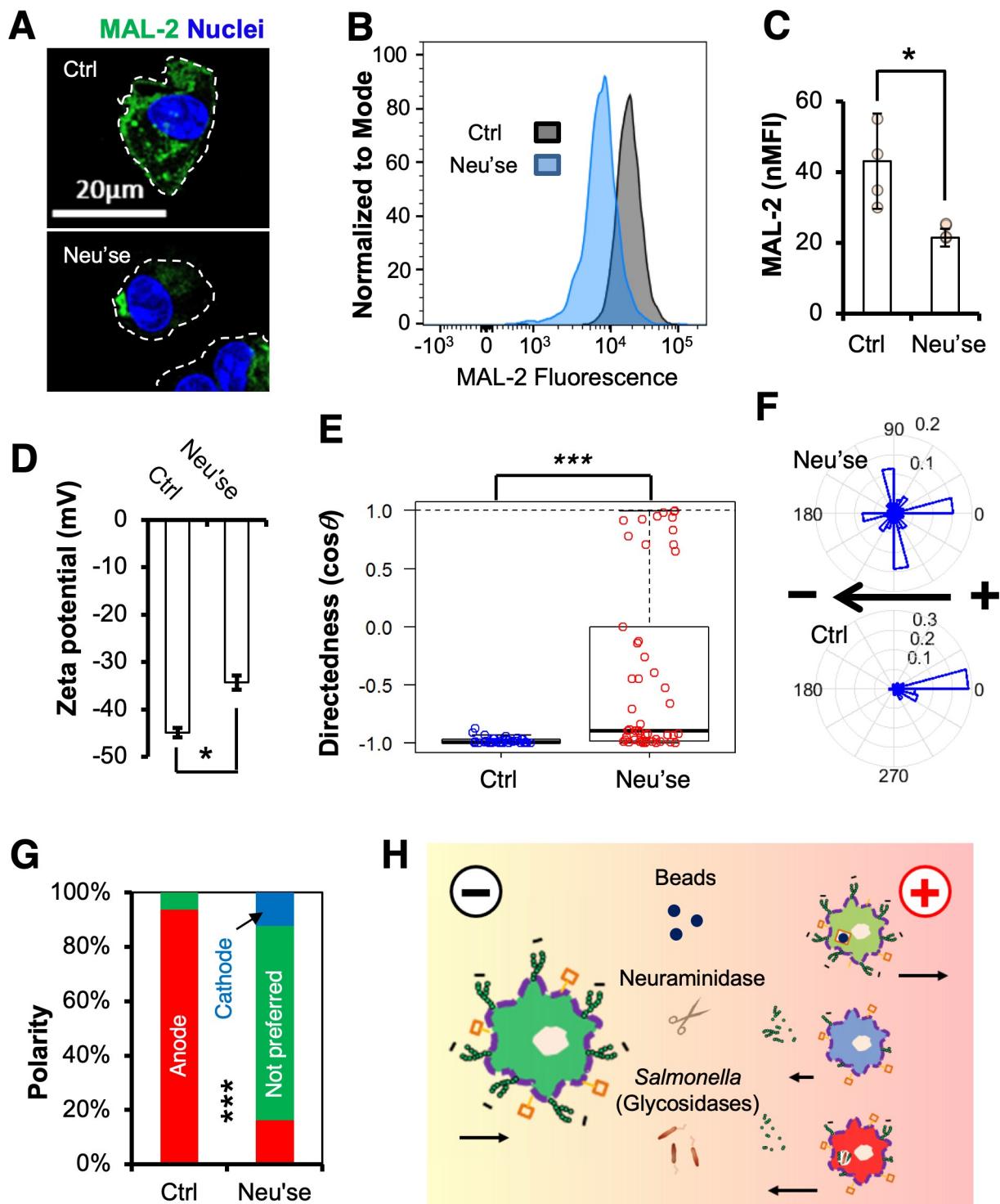
Fig 5. Cleavage of negatively charged sialic acids impairs macrophage galvanotaxis. (A) Representative confocal images of surface MAL-2 (green) of BMDMs incubated with 0 (Ctrl) or 100 mU ml^{-1} Neu'se for 30 min. Nuclei were counterstained with DAPI (blue). Bar, 20 μm. (B) Representative flow cytograms and (C) independent data of standardized MAL-2 fluorescence (green) intensity of BMDMs incubated with 0 or 100 mU ml^{-1} Neu'se for 30 min. $^{*}P < 0.05$ by Student t test. (D) Zeta potential of BMDMs incubated with 0 or 100 mU ml^{-1} Neu'se for 30 min. Data were quantified from a representative of 3 independent experiments. $^{*}P < 0.05$ by Student t test. (E) Directedness, (F) rose plots, and (G) polarity of BMDMs treated with or without Neu'se, followed by 3 h exposure to an EF of 4 V cm^{-1}. Data were quantified from a representative of 4 independent experiments. $^{***}P < 0.001$ by Student t test (Panel E). $^{***}P < 0.001$ by χ^2 test (Panel G) (See S1 Data). (H) Proposed model of *Salmonella*-infection–dependent directional switch in macrophage galvanotaxis. Upon exposure to an IGEF-like EF (marked gradient),

negatively charged (sign with small green circles) macrophages undergo robust directional migration to the anode. Phagocytosing *Salmonella* reduces surface negativity of the macrophage through catalytic activities of certain glycosidases, as exemplified by the cleavage of sialic acids with Neu'se (scissors). Consequently, activated macrophages can either undergo defective directional migration or switch direction to the cathode. Macrophages that phagocytosed beads through binding of nonsialylated surface components (brown squares) still migrate to the anode. Arrows indicate both direction and strength of macrophage galvanotaxis. BMDM, bone marrow-derived macrophage; cosθ, cosine theta; Ctrl, control; EF, electric field; IGEF, infection-generated electric field; MAL-2, Maackia Amurensis lectin II; Neu'se, neuraminidase; nMFI, normalized mean fluorescence intensity; ns, nonsignificant.

at least 51 putative glycosidases that likely function in glycan degradation [84]. In fact, a recent study identified several glycosidases, including a putative neuraminidase, as new virulence factors essential for *Salmonella* infection of epithelial cells, which is again independent of the SPI-1 [85]. We are in the process of performing genetic knockouts to identify the factors involved.

It is also possible that modification of surface glycan and reduction of zeta potential were mediated by internalization during phagocytosis of the bacterium itself rather than by bacterial enzymatic activities. For example, macrophages express Toll-like receptors (TLRs) that recognize structurally conserved molecules derived from *Salmonella* and other pathogens. All TLRs contain *N*-linked glycosylation consensus sites, and both TLR2 and TLR4 require glycosylation for surface translocation and function [86,87]. Binding of *Salmonella* to these glycosylated receptors and subsequent internalization may reduce surface negativity of macrophages, leading to directional switch under an EF. This idea is supported by our observations in which the accumulation of certain lectin binding aggregates within macrophages infected by *Salmonella* but not in cells challenged by microspheres (S8 and S9 Figs). It is also possible that a macrophage can uptake microspheres without significantly changing its zeta potential (e.g., through a neutralized receptor) and thus still migrate to the anode.

Disseminated *Salmonella* infection is a major health problem of developing countries, responsible for approximately 433,000 deaths annually [88]. Understanding the mechanisms that trigger dissemination is critical for efforts to target this key process for preventive and therapeutic purposes. We propose that macrophages are attracted to the site of infection by a combination of chemotaxis and galvanotaxis, driving the cells in the same direction. After phagocytosis of bacteria, surface electrical properties of the macrophage change, and galvanotaxis directs the cells away from the site of infection (Fig 6). Our study represents a new perspective for the initiating mechanisms, suggesting that *Salmonella* disseminates through infection-generated bioelectrical control of macrophage trafficking. It is important to emphasize that the demonstrated bidirectional migration of macrophages to the IGEF-like EFs is not a physical electrophoresis (movement of charged particles under direct-current EF) but rather a complex yet poorly understood biological process that requires phosphoinositide 3-kinases and other critical signaling activities, as well as the cellular motility machinery [25,81]. It is also worth emphasizing that the model proposed in this work is not mutually exclusive with respect to chemotaxis but offers an alternative and/or complementary mechanism of directional migration. Both directional cues can coexist and play equally important roles in orchestrating the initial stage of the innate immune response against bacterial infection (Fig 6), although a chemical gradient could be overridden by a strong electrical stimulus [59,89]. Both chemotaxis and galvanotaxis likely share critical signaling pathways as suggested in studies of macrophage-like *Dictyostelium*, which are highly sensitive to cyclic adenosine monophosphate gradients, as well as to electrical potential gradients [90–92]. Future work utilizing transgenic animals and pharmacological perturbations to target specific pathways (known or unknown) will help to pinpoint key molecules mediating the infection-dependent directional reversal (i.e., the molecular mechanisms to initiate disseminated infection) and response to bioelectric signaling.
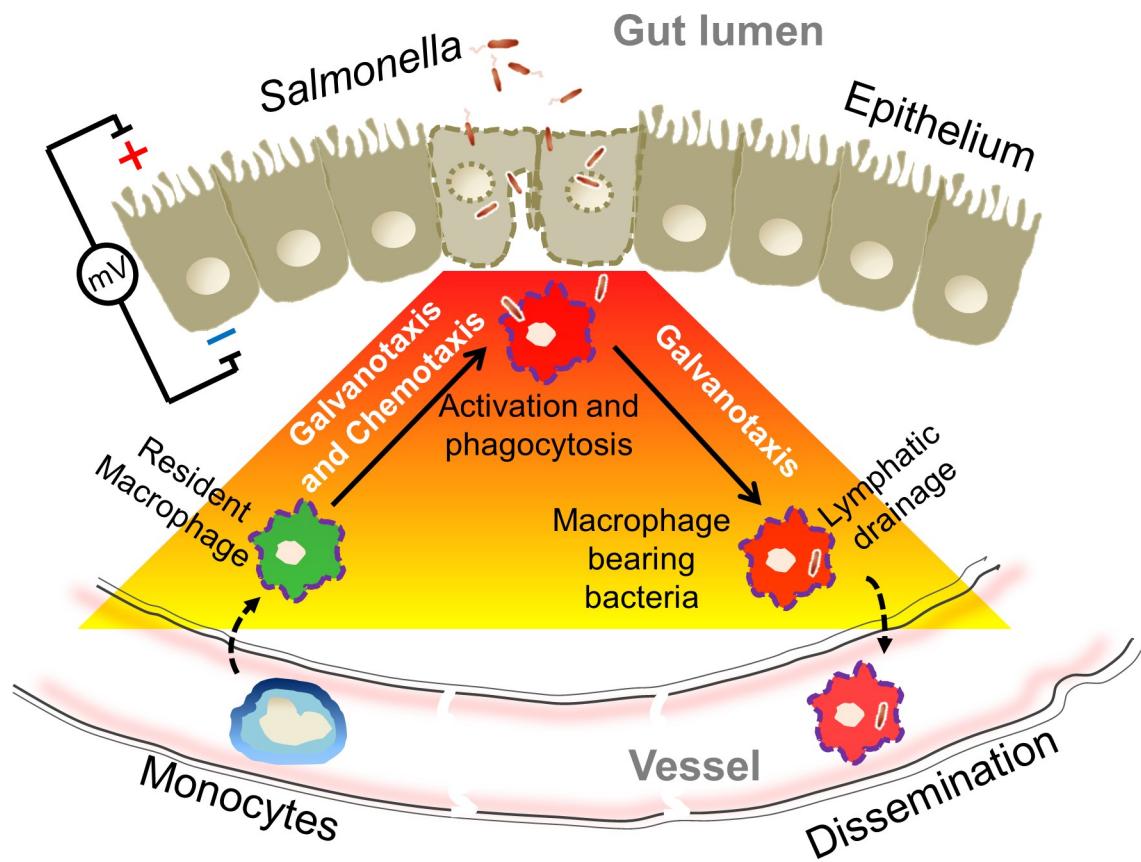
Fig 6. IGEF at gut epithelium and model of macrophage galvanotaxis in initiating dissemination. *Salmonella* invades and disrupts gut epithelial integrity, preferentially at the FAE, generating an IGEF (red to yellow gradient) that recruits resident macrophages to the bacteria entry sites—alone or synergistically with chemotaxis. Macrophages invaded by *Salmonella* revert galvanotaxis direction through the modification of surface electric properties to reach the lymphatic drainage and/or bloodstream, thus initiating dissemination. FAE, follicle-associated epithelium; IGEF, infection-generated electric field.

https://doi.org/10.1371/journal.pbio.3000044.g006

Triggering bacterial dissemination mediated by macrophage galvanotaxis might be a common strategy, not only for pathogenic *Salmonella* but also for other bacterial pathogens that are able to invade macrophages and survive intracellularly. Although the present work deals primarily with gut epithelium and enteric bacteria, the general mechanism that emerged from this work could also apply to other mucous epithelia such as the respiratory tract and its associated pathogens, e.g., *Mycobacterium tuberculosis* (the causative agent of tuberculosis) [93], which is another major public health concern.

Materials and methods

Mice and surgery

The mouse strains used were in a C57BL/6 background (both male and female mice were used in experiments). Mice were purchased from Jackson lab and maintained under a strict 12-h light cycle and given a regular chow diet in a specific pathogen-free facility at University of California (UC), Davis. All animal experiments were performed in accordance with regulatory guidelines and standards set by the Institutional Animal Care and Use Committee of UC Davis. In brief, we dissected mouse cecum following euthanasia and opened longitudinally along the mesenteric attachment remnant to avoid incision damage to the single Peyer's patch

located under the antimesenteric mucosa near the apex (S1A Fig). After thorough washing in mouse Ringer's solution (154 mM NaCl, 5.6 mM KCl, 1 mM $MgCl_2$, 2.2 mM $CaCl_2$, 10 mM glucose, and 20 mM HEPES [pH 7.4]) to remove the luminal contents, we placed the cecum with mucous side facing up, on a 30° slope of silicone gel prepared from polydimethylsiloxane (PDMS) in custom-made measuring chambers. The cecum was aligned and immobilized with fine metal (tungsten) pins prior to taking measurements (S1B Fig). This process was usually completed within 5 min.

Measuring TEP with glass microelectrodes

We used glass microelectrodes to directly measure the TEP of intestinal epithelium as previously described [28,94]. TEPs were recorded by microelectrode impalement through the epithelial layers. Microelectrodes (1–2 µm tip diameter; NaCl 3 M electrolyte) had resistances of approximately 1 to 2 MΩ, and the potentials were offset to 0 mV prior to impalement. Cecal FAE and adjacent villus epithelium were discriminated under a dissecting microscope within a Faraday cage on an antivibration table. In some cases, the TEP were measured as follows: first at the epithelial surface (0 µm), then stepwise at 50, 100, and 200 µm in depth, controlled by a micromanipulator (S2A Fig). The potential typically returns to the baseline of 0 mV after microelectrode withdrawal. If the reference baseline was $> \pm 1$ and $\leq \pm 5$ mV, the value was subtracted from the TEP recorded as shown in the equation (S2B Fig); if $> \pm 5$ mV, the trace was rejected. As a control, we measured the TEP of serosa epithelium and the TEP of formalin-fixed mucous epithelium. Measurements were performed at room temperature in mouse Ringer's solution. Data were acquired (saturated sampling at 100 Hz) and extracted using pClamp 10 (Molecular Devices) and analyzed using Excel (Microsoft, Redmond, WA).

Measuring ionic currents with vibrating probes

We used noninvasive vibrating probes to measure the electric current density (J_I) in µA cm^{-2} of mouse cecum epithelium as previously described [28,41,42]. The probes, platinum-electroplated at the tip (approximately 30 µm ball diameter), vibrated at a frequency between 100 and 200 Hz. Prior to measurements, the probe was calibrated to the experimental conditions by an applied J_I of 1.5 µA cm^{-2} (S3C Fig). Under a dissecting microscope, mounted mouse ceca were positioned in the nonconductive measuring chamber (S3A Fig). The plane of probe vibration was perpendicular to the epithelial surface at a distance as close as possible (S3B Fig). J_I was recorded until the plateau peak was reached (<1 min) (S3C Fig). Reference values were recorded with the probe away from the epithelium surface ($\gg$1 mm) (S3A Fig). Measurements were taken at room temperature in mouse Ringer's solution. During calibrations and measurements, a Faraday "wall" (grounded aluminum-wrapped cardboard) covered the microscope. As a control, we measured J_I near the surface of serosal epithelium and formalin-fixed mucous epithelium. Data were acquired and extracted using WinWCP V4 (Strathclyde Electrophysiology Software, University of Strathclyde, Glasgow, United Kindom) and analyzed using Excel (Microsoft, Redmond, WA).

Reagents, plasmids, and *Salmonella* strains

Special reagents used in this work are listed in S2 Table. Plasmids and *Salmonella* strains used in this work are listed in S3 Table. Cultures of *Escherichia coli* (for plasmid extraction) and *S.* Typhimurium were incubated aerobically at 37°C in Luria-Bertani (LB) broth (per liter: 10 g tryptone, 5 g yeast extract, 10 g NaCl) or on LB agar plates (1.5% Difco agar) overnight. Antibiotics were used at the following concentrations unless stated otherwise: 30 µg ml^{-1}

chloramphenicol, 50 µg ml^{-1} nalidixic acid, 100 µg ml^{-1} ampicillin, 50 µg ml^{-1} kanamycin, and 10 µg ml^{-1} tetracycline.

Construction of *S.* Typhimurium expressing fluorescent proteins

In an effort to monitor live intracellular *Salmonella* during macrophage galvanotaxis we constructed an *S.* Typhimurium strain derived from IR715 that constitutively expresses mCherry coded in its genome [95]. In brief, the *glmS*::*mCherry* allele was transferred to IR715 via P22 transduction from the donor strain *S.* Typhimurium SL1344St (a gift from Leigh Knodler) [96] and selected by chloramphenicol. To remove the FRT-flanked chloramphenicol cassette, the transductant was transformed with pCP20 encoding FLP recombinase. The resulting strain constitutively expressing mCherry encoded by *glmS*::*mCherry*::*FRT* was designated KLL18.

The GFP-expressing SPI-1 mutant Δ*invA* was generated by electroporating pGFT/RalFc into AJB75 [69]. The plasmid pGFT/RalFc was constructed in 2 steps. First, a fragment of a *gfp-mut3* gene under the control of the constitutively active kanamycin-resistance gene *aphA3* promoter was amplified from pJC43 [97] with the primers GFPmut3-F (5′- AGAGCTCCAGC GAACCATTTAAGGTGATAG -3′) and GFPmut3-R (5′- ACTGCAGTTATTTGTATAGTTC ATCCATGCC -3′). This fragment was then digested with SacI/PstI and cloned into pFT/ RalFc, a low–copy-number plasmid based on pBBR1-MCS4 [98].

Oral infection in a mouse model of human typhoid fever

The mouse is a well-established animal model for studying *Salmonella* pathogenesis [35]. C57BL/6 and other mice carrying a mutation in *nramp1* develop disseminated infections when challenged by *S.* Typhimurium, which mimics human typhoid fever [99]. For the mouse infection experiment, we used the hyper-disseminative D23580 strain [100,101]. In brief, D23580 was used to inoculate LB broth and incubated overnight at 37˚C. C57BL/6 mice (6 to 10 wk old, mixed sexes) were intragastrically infected with 10^9 bacteria (actual inoculum was determined by plating) in 0.1 ml LB broth. Uninfected mice used as a control were given 0.1 ml sterile LB broth in place of *Salmonella*.

Mice were euthanized at 16 h and 40 h post infection (PI) by CO_2 asphyxiation followed by cervical dislocation as the secondary method of euthanasia. The 16 h PI was chosen based on previous studies showing that the best-characterized route for the phagocytes harboring *Salmonella* to reach the bloodstream normally requires between 12 and 20 h [17,102]. MLNs and spleens were collected aseptically and homogenized in phosphate-buffered saline (PBS) for CFU enumeration. Ceca were dissected, cleaned, and then either mounted for bioelectrical measurement, prepared for histopathological fixation, or homogenized in PBS for CFU enumeration.

Histology

Ceca were fixed in 10% neutral buffered formalin. After fixation, tissues were routinely processed, embedded in paraffin, sectioned, and stained with hematoxylin–eosin.

Isolation and culture of primary mouse PMs and BMDMs

Both PMs and BMDMs were isolated from C57BL/6 mice (6 to 10 wk old, mixed sex) following standard procedures as previously described [103]. PMs were seeded onto 6-well plates and allowed to adhere to the plastic for 1 to 2 d in DMEM (Invitrogen) with 10% fetal bovine serum (Invitrogen) and 1× antibiotic-antimycotic solution (Invitrogen). BMDMs were cultured in the same medium as described above but supplemented with 20% L-929 conditioned

medium for 6 d (plus an extra feed at day 3), followed by 1-d culture without the conditioned medium. Adherent macrophages were then harvested by gently scraping with a "policeman" cell scraper and used for subsequent experiments accordingly. Cell viability was determined by trypan blue staining and counting.

Our initial galvanotaxis experiments were carried out in PMs. Because we observed better directional switch in BMDMs infected by *Salmonella* (S5 Fig), subsequent experiments were done in BMDMs, unless stated otherwise.

Gentamycin protection assay to determine intracellular bacteria CFU

The gentamycin protection assays were carried out as previously described [104]. In 24-well tissue culture-treated plates, 2×10^5 cells were seeded per well for 5 to 6 h in culture medium (DMEM with 10% fetal bovine serum and no antibiotics). *Salmonella* were grown overnight and used to infect macrophages at an MOI of 20. After 60 min of incubation, cells were gently washed 3× with PBS and further incubated in gentamycin-containing culture media at a final concentration of 50 μg ml^{-1} for an additional 60 min. Afterwards, media were replaced with culture media containing 10 μg ml^{-1} gentamycin for the duration of the experiment. Intracellular CFU was measured at 16 h PI. To measure intracellular CFU, macrophages were lysed using 0.5% Tween 20 for 5 min at room temperature and released by scraping with 1 ml pipette tips. CFUs were enumerated by plating.

Infection, challenge, and treatment of macrophages

Typically, 4×10^4 primary mouse macrophages were seeded per well of engineered silicon stencils sealed in custom-made EF chambers (see "Engineering silicone stencil and EF chamber design" for details) or 96-well glass bottom plates (Nunc) or 2×10^5 cells per well in 24-well tissue culture-treated plates depending on different experiment needs for 5 to 6 h in culture medium. Overnight cultures of *Salmonella* or fluorescently labeled microspheres were used to infect and/or challenge macrophages at an MOI of 20. The rest of the procedures were similar to the gentamycin protection assay. Cells were cultured in medium containing 10 μg ml^{-1} gentamycin for 16 h, and subsequent galvanotaxis experiments were carried out in the same medium containing gentamycin.

For the neuraminidase treatment, cells were incubated in culture medium containing 100 mU ml^{-1} neuraminidase from *Vibrio cholerae* (Sigma-Aldrich) for 30 min at 37˚C [70]. Cells were then washed with culture medium, and subsequent galvanotaxis experiments were carried out in the culture medium containing no neuraminidase.

For the low pH experiments, cells were incubated in culture medium of pH 5.8 buffered with 15 mM MES (Sigma-Aldrich) for 60 min, and subsequent galvanotaxis experiments were carried out in the same media of pH 5.8 [81]. Control experiments were carried out always in parallel in culture medium of pH 7.4 buffered with 14.4 mM HEPES (Invitrogen).

Galvanotaxis assay

1. Engineering silicone stencil and EF chamber design. We have tested cover glass and plastics coated with different substrates and found that macrophages perform robust and consistent galvanotaxis when cultured in tissue culture dishes (Corning). Therefore, our EF chambers were customized based on 100 mm tissue culture dishes. To facilitate group comparability and EF control, we engineered removable and reusable silicone stencils of multiple wells (diameter of 8 mm, thickness of 2.4 mm) to seed the same batch of cells that can be challenged and/or treated with different bacteria and/or substances and monitored under identical

galvanotactic conditions simultaneously [105]. The EF tunnel height is fixed at around 120 μm by double-sided silicone tapes cut by a computer-controlled laser cutter [80].

2. EF application and time-lapse recording. We applied exogenous EF as previously described [42,105–107]. The EF strength is based on the IGEF we measured at the gut epithelium in 2 ways. First, we detected an inward J_I of approximately 1.5 μA cm^{-2} at *Salmonella*-infected FAE. The mouse Ringer's solution we used in the measurement has a resistivity (ρ) of 19.47 mΩ cm, measured with a conductivity meter. A common approximation to the current density assumes that the current is simply proportional to the EF, as expressed by the following equation (derived from Ohm's law):

$$J_I = \frac{E}{\rho}, \tag{1}$$

where E is the EF. Plugging J_I and ρ into the equation, we calculated that a density of 1.5 μA cm^{-2} equals an EF of 0.77 V cm^{-1}. Based on trials in rabbit corneal epithelium, the in vivo J_I is likely 2 to 4 times larger than the ex vivo J_I because of the higher resistances of the tissues and of the higher physiological temperature. Second, we detected a TEP of approximately 25 mV crossing a single layer of *Salmonella*-infected gut epithelium. This generates an EF of 5 V cm^{-1} providing an epithelial cell height of 50 μm. After testing a range around those values, we have empirically chosen an EF of 4 V cm^{-1} because it consistently induced significant directional migration of primary mouse macrophages, although biased directional migration can be achieved by an EF as small as 0.5 V cm^{-1}. Actual EF strengths were measured and determined with a voltmeter before and after each EF application.

Cell migration was monitored with a Carl Zeiss Observer Z1 inverted microscope equipped with a motorized stage and an incubation chamber (37˚C and 5% CO$_2$). Time-lapse contrast images and/or images of appropriate fluorescence channels were captured using MetaMorph NX program (Molecular Devices). A Retiga R6 (QImaging) scientific CCD camera and long exposure time (approximately 2 s) were used to detect and monitor intracellular *Salmonella* expressing fluorescent proteins. Typically, in each experiment, 2 to 4 fields of each condition under a 10× or a long-distance 20× lens were chosen. Images were taken at 5-min intervals for up to 3 h unless stated otherwise.

3. Image processing and data analysis and/or presentation. Time-lapse images were imported, processed, and assembled in ImageJ (http://rsbweb.nih.gov/ij). To quantify single-cell and population motility, we extracted the trajectory of each cell migration (>30 cells for each condition) using an automatic and/or manual tracking tool [42,81,105]. Directionality as directedness in cosine theta (cosθ), in which θ is the angle that each cell moved with respect to the EF vector, was quantified from the coordinates of each trajectory [108,109]. If a cell moved perfectly along the field vector toward the cathode, the cosine of this angle would be 1; if the cell moved perpendicular to the field vector, the cosine of this angle would be 0; and if the cell moved directly toward the anode, the cosine of this angle would be −1. Dead cells (macrophages killed by *Salmonella*) or cells unresponsive to the EF (due to neuraminidase treatment or acidic conditions) were either washed away or excluded from quantification by migration speed thresholding. The thresholds were estimated from fixed cells recorded in the same optical parameters and experiment setting for the live macrophages. The galvanotaxis assays and quantification of directionality in BMDMs infected with *ΔinvA* and their isogenic WT *Salmonella* were assigned in a double-blinded manner.

To simulate cell migration, each cell was numbered and its *x* and *y* coordinates were measured on the first image and on every subsequent image in the image stack, with the x-axis parallel to the applied EF. The (*x*, *y*) data of each cell were imported with the ImageJ chemotaxis tool plugin and recalculated based on the optical parameters (lens and camera). Trajectories of

the cells in each group were simulated in a Cartesian coordinate system by placing the first coordinates of each cell in the origin (0, 0).

To plot the rose histograms, we combined θ of each time interval of tracked cells in each group. The vector θ, expressed in radians, was calculated from the coordinates of each trajectory. The distribution of θ in 12 angle bins and their abundance in percentage were plotted in Matlab (Mathworks, Natick, MA) using a custom script (available upon request).

4. Morphological analysis. The polarity of macrophages was determined by the relative distribution of the characterized protrusive lamellipodia front and uropod tail with respect to the applied EF. These were done by visually inspecting a large number of cells (>50 cells in each case) from images taken at 3 h after EF exposure or by quantifying cellular actin intensity of confocal images using ImageJ software with line scan and color function plugins [105].

Immunobiochemistry, lectin staining, and confocal microscopy

Macrophages were seeded in either 96-well glass bottom plates or custom-made EF chambers and infected, challenged, and/or treated by following procedures as described above. The cells were fixed with 4% paraformaldehyde immediately or after EF exposure for 3 h with field orientation marked. *Salmonella* were detected with a polyclonal antibody specific to *Salmonella* spp. (Mybiosource, San Diego, CA) stained by an Alexa Fluor 488-conjugated secondary antibody. F-actin was labeled by Alexa Fluor 555 Phalloidin. Nuclei were labeled by Hoechst 33342.

In the cases of lectin staining, fixed cells were incubated with FITC-labeled lectin (S1 Table) overnight at 4˚C, washed extensively, and then stained with DAPI for 10 min on ice.

Cells were photographed using either an inverted (for cells on cover glass with no EF) or an upright (for cells on plastic EF chambers) Leica TCS SP8 confocal microscope (Leica microsystem). Images were processed using ImageJ. Quantification and comparison of fluorescent intensity were done in images taken in the same batch with the same optical setup and parameters. Lectin binding aggregates stained after permeabilization were quantified by thresholding. Cells were counted using particle analysis function.

Flow cytometry

Infected, challenged, and/or treated macrophages, handled according to the procedures described above, were then incubated with Fc-block (BD, Franklin Lakes, NJ) on ice for 15 min, stained with FITC-labeled lectin (S1 Table) for 1 h on ice, and then stained with Aqua-LIVE/DEAD (Invitrogen, Carlsbad, CA) for 30 min at room temperature. Cells were washed after each step and before being analyzed on a BD Fortessa flow cytometer. Data were analyzed using FlowJo software (Tree Star Inc. Ashland, OR). After gating single cells and live cells, the geometric mean fluorescence intensity and standard error (SE) were collected for each FITC lectin in each condition in addition to Fluorescence Minus One (FMO) for FITC-lectin (no FITC-lectin staining). The geometric mean fluorescence intensity was then standardized across experiments using the following equation:

$$x_{FMO}(MFI) = \frac{x(MFI) - FMO(MFI)}{FMO(SD)}, \tag{2}$$

where $x_{FMO}(MFI)$ is the standardized geometric mean fluorescence intensity of a specific lectin for a specific experiment, $x(MFI)$ is the geometric mean fluorescence intensity of a specific lectin for a specific experiment, $FMO(MFI)$ is the geometric mean fluorescence intensity of the FMO for a specific experiment, and $FMO(SD)$ is the standard deviation of the FMO for a

specific experiment. Standardized geometric mean fluorescent intensities were then plotted and tested for statistical significance (S10 Fig).

Measuring zeta potential

Macrophages were seeded onto 24-well tissue culture plates and infected, challenged, and/or treated following procedures as described above. Cells were fixed in 2% paraformaldehyde and washed with motility buffer (10^{-4} M potassium phosphate buffer at pH 7.0, with 10^{-4} M EDTA) [56]. Cells were then gently collected by scraping with a "policeman" cell scraper, and subsequent measurements were done in motility buffer, except for the macrophages tested for acidic treatment, which were measured in either pH 5.8 medium or pH 7.4 medium as a control. Zeta potential was determined by electrophoretic light scattering at 25˚C with a Zetasizer (Malvern Panalytical Ltd, Malvern, United Kingdom). Zeta potential was calculated in mV, and differences between groups were analyzed by Student t test.

Statistics

Galvanotaxis data from representatives of at least 4 independent experiments were routinely presented as mean ± SE, unless stated otherwise. Distributions of macrophage polarity between control and neuraminidase treated or between neutral and acidic conditions were analyzed using χ^2 test. Student t test and one-way ANOVA analysis followed by post hoc Tukey HSD test were used for paired or unpaired comparisons among 2 groups or multiple groups (more than 2), respectively.

Supporting information

S1 Table. Selected lectins used in this study.
(DOCX)

S2 Table. Special reagents used in this study.
(DOCX)

S3 Table. Plasmids and *Salmonella* strains used in this study.
(DOCX)

S1 Fig. An ex vivo mouse cecum model for characterization of bioelectrical activities of gut epithelium. (A) Cecum was dissected from C57BL/6 mouse and opened longitudinally along the mesenteric attachment remnant (dotted white line) to avoid incision damage of lymphatic structure that is located under the antimesenteric mucosa near the apex (red circle). (B) Cecum mounted in a custom-made chamber with mucous epithelium facing up on a 30˚ slope of silicone gel and held with the cecum edge with fine metal pins (white arrow heads). (C) Mouse cecal epithelium under a dissecting microscope. FAE—the smooth appearing regions (f), and inter-follicle/surrounding villi (v) are shown. Bar, 5,000 μm. (D) HE stain of a mouse cecum showing the structure of a Peyer's patch. Bar, 200 μm. (E) Magnification of the checked area of panel D showing FAE and inter-follicle and surrounding villi. Double-dotted forks indicate the sites where TEP and J_I were measured. Serosal epithelia served as controls. Bar, 100 μm. FAE, follicle-associated epithelium; HE, hematoxylin–eosin; J_I, electric current density; TEP, transepithelial potential. (TIF)

S2 Fig. Measuring TEP with microelectrodes. (A) Schematic depicting the microelectrode setup, sites, and procedures of measurement. The measuring microelectrode was impaled through the FAE or surrounding villus epithelial layer (one site at a time), and the circuit was closed by a reference electrode placed in the buffer, representing the lumen. Microelectrode

resistance (S, in which 10 mV equals 1 MΩ) was generated and recorded prior to each impalement to ensure that the tip was neither broken nor obstructed. In some cases, the TEP of infected FAEs were measured as follows: first at the epithelial surface (0 μm), then in stepwise at 50, 100, and 200 μm in depth. The potential typically returns to the baseline of 0 mV after microelectrode withdrawal (W). (B) Two representative traces and a specific equation used to calculate TEP value as a modified mean from S1 Data. In the equation, "a" and "b"'are the early and late values of each impalement in which the electrode was kept in position for at least 60 s. "c" is the reference value immediately after the electrode withdrawal. FAE, follicle-associated epithelium; TEP, transepithelial potential.
(TIF)

S3 Fig. Measuring bioelectric currents using vibrating probes. (A) Schematic of equipment setup and measuring procedures. Under a dissecting microscope, a probe vibrating between 100 and 200 Hz controlled by a micromanipulator is moved from the reference position (R) to the measuring position (M), as close as possible (approximately 20 μm) to the epithelial surface, to detect ionic currents. (B) A picture of a vibrating probe approaching an FAE. (C) Representative traces of bioelectric current measured at the FAE from *Salmonella*-infected or mock-infected control mouse cecum. Probes were calibrated by passing a 1.5 μA cm^{-2} electric current through the measuring buffer in either direction (see S1 Data). By convention, flux of positive charge is used for electric current direction. As in most studies, we used conventional current flow; therefore outward current density is defined as net positive charge leaving the epithelial surface and inward current densities as that entering. Hence, positive values represent net outward current densities, and negative values represent net inward current densities. FAE, follicle-associated epithelium.
(TIF)

S4 Fig. Invasion of cecal epithelium and early dissemination. (A) Ceca, free of contents, MLNs and spleens were dissected in sterile conditions at 16 h or 40 h PI from mice orally infected with *S.* Typhimurium. Bacterial loads were determined by homogenizing each specimen, serial dilution and plating on LB plates. CFUs were calculated by counting bacterial colonies selected with appropriate antibiotics. CFUs lower than the detection limit as indicated by the dotted line were treated as the limit (see S1 Data). (B) HE stain of a cecum section from mice orally infected with *S.* Typhimurium. Disruption of the FAE (arrowhead) and thickened intestinal wall are shown. Bar, 100 μm. CFU, colony forming unit; FAE, follicle-associated epithelium; HE, hematoxylin–eosin; LB, Luria-Bertani; MLN, mesenteric lymph node; PI, post infection; *S.* Typhimurium, *Salmonella enterica* serotype Typhimurium.
(TIF)

S5 Fig. Robust cathodal direction switch in BMDMs infected with different virulent *Salmonella* strains. Mouse BMDMs challenged with 3 virulent *S.* Typhimurium at an MOI of 20, subject to galvanotaxis assay at 16 h PI. EF is 4 V cm^{-1}. Duration is 3 h. (A) Pie charts show percentage of cells migrating to the cathode (red) or to the anode (blue). (B) Overall directionality. $^{**}P < 0.01$ by one-way ANOVA analysis followed by post hoc Tukey HSD test (see S1 Data). (C) Quantification of intracellular bacteria. BMDMs were seeded in 24-well plates and challenged with *S.* Typhimurium at an MOI of 20. Actual inocula were determined by plating and colony counting. Intracellular bacteria at 16 h PI was determined by a gentamycin protection assay. Representative data are presented as log CFU per well, normalized to each inoculum. Bar in SE from triplicate wells (see S1 Data). BMDM, bone marrow-derived macrophage; CFU, colony forming unit; EF, electric field; HSD, honest significant difference; MOI, multiplicity of infection; ns, nonsignificant; PI, post infection; *S.* Typhimurium, *Salmonella enterica*

serotype Typhimurium.
(TIF)

S6 Fig. Determining challenge and/or infection rates by flow cytometry. BMDMs were challenged with 1-μm, red fluorescently labeled polystyrene microspheres or live *S*. Typhimurium IR715 constitutively expressing mCherry at an MOI of 20. Excessive beads and bacteria were removed by washing. Residual extracellular bacteria were killed per gentamycin treatment. (A–E) Representative flow cytograms of a complete experimental design to count target cells using flow cytometry. (A) At 16 h PI, cells were harvested and labeled with Aqua blue and analyzed by flow cytometry. (B) An example of gates used to exclude fragments and cell clumps. (C) Dead cells were excluded by gating Aqua blue signal. Live cells were subject to further cell counting in either PE fluorescence channel for red fluorescent beads (D) or with the dTomato fluorescence channel for *Salmonella* expressing mCherry (E). (F) Representative bar charts showing percentage of macrophages containing intracellular bacteria or beads. BMDM, bone marrow-derived macrophage; MOI, multiplicity of infection; PE, Phycoerythrin; PI, post infection; *S*. Typhimurium, *Salmonella enterica* serotype Typhimurium.
(TIF)

S7 Fig. Phagocytosis (of microspheres) per se does not affect directional migration of macrophages in response to EF. (A) BMDMs were seeded in 96-well glass-bottom plates and challenged with 1-μm microspheres with blue fluorescent at an MOI of 20. Excessive microspheres were removed by washing with medium. At 16 h PI, cells bearing beads (blue) were counted under an epifluorescence microscope. (B) Pie chart of percentage of cells with 0, 1, or up to 5 bead(s) in a typical experiment. (C) Trajectories and (D) directedness of macrophages under an EF of 4 V cm^{-1} in the indicated orientation for 3 h. ns by unpaired Student *t* test (see S1 Data). BMDM, bone marrow-derived macrophage; EF, electric field; MOI, multiplicity of infection; ns, nonsignificant; PI, post infection.
(TIF)

S8 Fig. GNL-binding aggregates in macrophages infected with *Salmonella*. Representative confocal photographs show BMDMs containing red fluorescence-labeled beads or *Salmonella* expressing mCherry (red). Cells were fixed, permeabilized, and stained with DAPI (blue) and FITC-conjugated GNL (green). Cells were outlined in merged photographs (white dashed line). Bar, 20 μm. Note the GNL-binding aggregates inside macrophages containing intracellular *Salmonella* (white arrowhead). BMDM, bone marrow-derived macrophage; FITC, fluorescein isothiocyanate; GNL, Galanthus Nivalis lectin.
(TIF)

S9 Fig. Con A–binding aggregates in macrophages infected by *Salmonella*. (A) Galvanotaxis assays were performed per the rigorous experiment design illustrated in Fig 3A. BMDMs were fixed, permeabilized, and labeled with Alexa Fluor 555 Phalloidin (red) and FITC-conjugated Con A (green), and scanned with an upright confocal microscope. Phagocytosed beads and intracellular bacteria were pseudocolored in yellow. Bar, 20 μm. Control macrophages (left panel) and macrophages challenged with beads (middle panel) were exclusively polarized to the anode with a characteristic morphology: massive actin meshwork in the front and a uropod at the rear. Cells infected with *Salmonella* (right panels) reversed their polarity to the cathode. Note the significant Con A–binding aggregates in macrophages containing intracellular *Salmonella* (white arrowheads). (B) Quantification of macrophages with Con A aggregates. Number of cells counted is indicated inside each bar. $^{***}P < 0.001$ by χ^2 test (see S1 Data). BMDM, bone marrow-derived macrophage; Con A, concanavalin A; FITC, fluorescein isothiocyanate.
(TIF)

S10 Fig. The effects of *Salmonella* infection and neuraminidase treatment on the binding of selected lectins. Box plots showing nMFI of macrophages, either (A) challenged with microspheres and *Salmonella* at 16 h PI or (B) incubated with 0 or 100 mU ml^{-1} neuraminidase for 30 min. Cells were stained with Con A, SNA, GNL, or RCA-1 and analyzed by flow cytometry. Data from 4 independent experiments. ns by unpaired Student *t* test (see S1 Data). Con A, concanavalin A; GNL, Galanthus Nivalis lectin; nMFI, normalized mean fluorescence intensity; ns, nonsignificant; PI, post infection; SNA, Sambucus Nigra lectin; RCA-1, Ricinus Communis Agglutinin I.
(TIF)

S11 Fig. Low pH reduces surface charge and impairs macrophage galvanotaxis. (A) Zeta potential of BMDMs cultured in pH 7.4 or pH 5.8. ***$P < 0.001$ by Student *t* test. (B) Rose plots and (C) directedness of BMDMs cultured in pH 7.4 or pH 5.8 exposed to an EF of 4 V cm^{-1} for 3 h. ***$P < 0.001$ by Student *t* test. (D) Polarity of BMDMs cultured in pH 7.4 or pH 5.8 and exposed to an EF of 4 V cm^{-1} for 3 h. Data were quantified from a representative of 2 independent experiments. ***$P < 0.001$ by χ^2 test (see S1 Data). See also S5 Movie. BMDM, bone marrow-derived macrophage; EF, electric field.
(TIF)

S1 Data. Raw data for graphing.
(XLSX)

S1 Movie. Galvanotaxis of primary mouse macrophages to the anode. Primary mouse PMs migrate to the anode in response to an EF of 4 V cm^{-1} in the indicated orientation for 5 h 50 min. Time-lapse phase contrast images were acquired 1 frame every 5 min. Bar, 50 μm. EF, electric field; PM, peritoneal macrophage.
(AVI)

S2 Movie. Bidirectional galvanotaxis of macrophages challenged with *Salmonella*. Unidirectional migration of PMs to the anode in control (top) (trajectories in highlighted yellow line) and bidirectional migration of macrophages challenged with *S.* Typhimurium (bottom), either to the cathode (trajectories in highlighted red line) or to the anode (trajectories in highlighted yellow line), under an EF of 4 V cm^{-1} in the indicated orientation for 3 h. Time-lapse phase contrast images were acquired 1 frame every 5 min. Bar, 50 μm. EF, electric field; PM, peritoneal macrophage; *S.* Typhimurium, *Salmonella enterica* serotype Typhimurium.
(AVI)

S3 Movie. Infection-dependent directional switch of macrophage galvanotaxis is SPI-1 independent. Galvanotaxis of control macrophages (BMDMs) (top left) or macrophages challenged with microspheres (bottom left) or WT *Salmonella* (bottom right) or SPI-1 mutant *ΔinvA* (top right), under identical conditions at an EF of 4 V cm^{-1} in the indicated orientation for 3 h. Time-lapse phase contrast and fluorescence images were acquired 1 frame every 5 min sequentially and combined using ImageJ. Note the opposite directional migration of macrophages containing beads (blue) or *Salmonella* (red and green) to the anode or to the cathode, respectively. Bar, 50 μm. BMDM, bone marrow-derived macrophage; EF, electric field; SPI-1, *Salmonella* pathogenicity island 1; WT, wild type.
(AVI)

S4 Movie. Treatment with neuraminidase severely impairs macrophage galvanotaxis. Impaired directional migration of BMDMs treated with neuraminidase (left), compared in parallel to the unidirectional migration of control macrophages (right) to the anode under an

EF of 4 V cm^{-1} in the indicated orientation for 2 h 45 min. Time-lapse phase contrast images were acquired 1 frame every 5 min sequentially and combined by using ImageJ. Bar, 100 μm. BMDM, bone marrow-derived macrophage; EF, electric field.
(AVI)

S5 Movie. Low pH impairs macrophage galvanotaxis. Galvanotactic behaviors of BMDMs cultured in acidic condition of pH 5.8 (top) compared, in parallel, to the unidirectional migration of macrophages cultured in pH 7.4 (bottom) to the anode, under an EF of 4 V cm^{-1} in the indicated orientation for 3 h. Time-lapse phase contrast images were acquired 1 frame every 5 min sequentially and combined using ImageJ. Bar, 100 μm. BMDM, bone marrow-derived macrophage; EF, electric field.
(AVI)

Acknowledgments

Author Contributions

Conceptualization: Yaohui Sun, Alex Mogilner, Min Zhao.

Data curation: Yaohui Sun, Fernando Ferreira, Guillaume Luxardi, Emanual Maverakis.

Formal analysis: Yaohui Sun, Brian Reid, Fernando Ferreira, Guillaume Luxardi, Kan Zhu, Gege Xu, Yuxin Sun.

Funding acquisition: Emanual Maverakis, Alex Mogilner, Min Zhao.

Investigation: Yaohui Sun, Brian Reid, Fernando Ferreira, Guillaume Luxardi, Li Ma, Kristen L. Lokken, Kan Zhu, Gege Xu, Yuxin Sun, Volodymyr Ryzhuk, Min Zhao.

Methodology: Yaohui Sun, Brian Reid, Carlito B. Lebrilla, Emanual Maverakis, Min Zhao.

Project administration: Yaohui Sun, Alex Mogilner, Min Zhao.

Resources: Kristen L. Lokken, Carlito B. Lebrilla, Emanual Maverakis, Alex Mogilner, Min Zhao.

Supervision: Carlito B. Lebrilla, Emanual Maverakis, Alex Mogilner, Min Zhao.

Validation: Yaohui Sun, Emanual Maverakis, Alex Mogilner, Min Zhao.

Visualization: Yaohui Sun, Brian Reid, Fernando Ferreira.

Writing – original draft: Yaohui Sun.

Writing – review & editing: Brian Reid, Fernando Ferreira, Betty P. Guo, Emanual Maverakis, Alex Mogilner, Min Zhao.

References

1. Mowat A.M., Anatomical basis of tolerance and immunity to intestinal antigens. Nat Rev Immunol, 2003. 3(4): p. 331–41. https://doi.org/10.1038/nri1057 PMID: 12669023

2. Jones B.D., Ghori N., and Falkow S., Salmonella typhimurium initiates murine infection by penetrating and destroying the specialized epithelial M cells of the Peyer's patches. J Exp Med, 1994. 180(1): p. 15–23. PMID: 8006579

3. Ohl M.E. and Miller S.I., Salmonella: a model for bacterial pathogenesis. Annu Rev Med, 2001. 52: p. 259–74. https://doi.org/10.1146/annurev.med.52.1.259 PMID: 11160778

4. Shi C. and Pamer E.G., Monocyte recruitment during infection and inflammation. Nat Rev Immunol, 2011. 11(11): p. 762–74. https://doi.org/10.1038/nri3070 PMID: 21984070

5. Serbina N.V., et al., Monocyte-mediated defense against microbial pathogens. Annu Rev Immunol, 2008. 26: p. 421–52. https://doi.org/10.1146/annurev.immunol.26.021607.090326 PMID: 18303997

6. Servant G., et al., Polarization of chemoattractant receptor signaling during neutrophil chemotaxis. Science, 2000. 287(5455): p. 1037–40. PMID: 10669415

7. Devreotes P.N. and Zigmond S.H., Chemotaxis in eukaryotic cells: a focus on leukocytes and Dictyostelium. Annu Rev Cell Biol, 1988. 4: p. 649–86. https://doi.org/10.1146/annurev.cb.04.110188.003245 PMID: 2848555

8. Hensel M., et al., Simultaneous identification of bacterial virulence genes by negative selection. Science, 1995. 269(5222): p. 400–3. PMID: 7618105

9. Ochman H., et al., Identification of a pathogenicity island required for Salmonella survival in host cells. Proc Natl Acad Sci U S A, 1996. 93(15): p. 7800–4. PMID: 8755556

10. Galan J.E., Salmonella interactions with host cells: type III secretion at work. Annu Rev Cell Dev Biol, 2001. 17: p. 53–86. https://doi.org/10.1146/annurev.cellbio.17.1.53 PMID: 11687484

11. Galan J.E. and Curtiss R. 3rd, Cloning and molecular characterization of genes whose products allow Salmonella typhimurium to penetrate tissue culture cells. Proc Natl Acad Sci U S A, 1989. 86(16): p. 6383–7. PMID: 2548211

12. Figueira R., et al., Identification of salmonella pathogenicity island-2 type III secretion system effectors involved in intramacrophage replication of S. enterica serovar typhimurium: implications for rational vaccine design. MBio, 2013. 4(2): p. e00065. https://doi.org/10.1128/mBio.00065-13 PMID: 23592259

13. Celli J., Surviving inside a macrophage: the many ways of Brucella. Res Microbiol, 2006. 157(2): p. 93–8. https://doi.org/10.1016/j.resmic.2005.10.002 PMID: 16364608

14. Chaurasiya S.K. and Srivastava K.K., Downregulation of protein kinase C-alpha enhances intracellular survival of Mycobacteria: role of PknG. BMC Microbiol, 2009. 9: p. 271. https://doi.org/10.1186/1471-2180-9-271 PMID: 20030858

15. Isberg R.R., O'Connor T.J., and Heidtman M., The Legionella pneumophila replication vacuole: making a cosy niche inside host cells. Nat Rev Microbiol, 2009. 7(1): p. 13–24. https://doi.org/10.1038/nrmicro1967 PMID: 19011659

16. Monack D.M., et al., Yersinia signals macrophages to undergo apoptosis and YopJ is necessary for this cell death. Proc Natl Acad Sci U S A, 1997. 94(19): p. 10385–90. PMID: 9294220

17. Vazquez-Torres A., et al., Extraintestinal dissemination of Salmonella by CD18-expressing phagocytes. Nature, 1999. 401(6755): p. 804–8. https://doi.org/10.1038/44593 PMID: 10548107

18. Pagan A.J. and Ramakrishnan L., Immunity and Immunopathology in the Tuberculous Granuloma. Cold Spring Harb Perspect Med, 2015. 5(9).

19. Helaine S., et al., Internalization of Salmonella by macrophages induces formation of nonreplicating persisters. Science, 2014. 343(6167): p. 204–8. https://doi.org/10.1126/science.1244705 PMID: 24408438

20. Shi R. and Borgens R.B., Embryonic Neuroepithelial Sodium-Transport, the Resulting Physiological Potential, and Cranial Development. Developmental Biology, 1994. 165(1): p. 105–116. https://doi.org/10.1006/dbio.1994.1238 PMID: 8088429

21. McCaig C.D., et al., Controlling cell behavior electrically: current views and future potential. Physiol Rev, 2005. 85(3): p. 943–78. https://doi.org/10.1152/physrev.00020.2004 PMID: 15987799

22. Levin M., Pezzulo G., and Finkelstein J.M., Endogenous Bioelectric Signaling Networks: Exploiting Voltage Gradients for Control of Growth and Form. Annu Rev Biomed Eng, 2017. 19: p. 353–387. https://doi.org/10.1146/annurev-bioeng-071114-040647 PMID: 28633567

23. Levin M. and Martyniuk C.J., The bioelectric code: An ancient computational medium for dynamic control of growth and form. Biosystems, 2018. 164: p. 76–93. https://doi.org/10.1016/j.biosystems.2017.08.009 PMID: 28855098

24. Barker A.T., Jaffe L.F., and Vanable J.W., The Glabrous Epidermis of Cavies Contains a Powerful Battery. American Journal of Physiology, 1982. 242(3): p. R358–R366. https://doi.org/10.1152/ajpregu.1982.242.3.R358 PMID: 7065232

25. Zhao M., et al., Electrical signals control wound healing through phosphatidylinositol-3-OH kinase-gamma and PTEN. Nature, 2006. 442(7101): p. 457–60. https://doi.org/10.1038/nature04925 PMID: 16871217

26. Nuccitelli R., A role for endogenous electric fields in wound healing. Curr Top Dev Biol, 2003. 58: p. 1–26. PMID: 14711011

27. Pai V.P., et al., Endogenous gradients of resting potential instructively pattern embryonic neural tissue via Notch signaling and regulation of proliferation. J Neurosci, 2015. 35(10): p. 4366–85. https://doi.org/10.1523/JNEUROSCI.1877-14.2015 PMID: 25762681

28. Ferreira F., et al., Early bioelectric activities mediate redox-modulated regeneration. Development, 2016. 143(24): p. 4582–4594. https://doi.org/10.1242/dev.142034 PMID: 27827821

29. Chiang M.C., Robinson K.R., and Vanable J.W., Electrical Fields in the Vicinity of Epithelial Wounds in the Isolated Bovine Eye. Experimental Eye Research, 1992. 54(6): p. 999–1003. PMID: 1521590

30. Allen G.M., Mogilner A., and Theriot J.A., Electrophoresis of cellular membrane components creates the directional cue guiding keratocyte galvanotaxis. Curr Biol, 2013. 23(7): p. 560–8. https://doi.org/10.1016/j.cub.2013.02.047 PMID: 23541731

31. Zhao Z., et al., Directed migration of human bone marrow mesenchymal stem cells in a physiological direct current electric field. Eur Cell Mater, 2011. 22: p. 344–58. PMID: 22125259

32. Lin F., et al., Lymphocyte electrotaxis in vitro and in vivo. J Immunol, 2008. 181(4): p. 2465–71. PMID: 18684937

33. Moriarty L.J. and Borgens R.B., The effect of an applied electric field on macrophage accumulation within the subacute spinal injury. Restor Neurol Neurosci, 1999. 14(1): p. 53–64. PMID: 12671271

34. Hoare J.I., et al., Electric fields are novel determinants of human macrophage functions. J Leukoc Biol, 2015.

35. Tsolis R.M., et al., Of mice, calves, and men. Comparison of the mouse typhoid model with other Salmonella infections. Adv Exp Med Biol, 1999. 473: p. 261–74. PMID: 10659367

36. Tsolis R.M., et al., How To Become a Top Model: Impact of Animal Experimentation on Human Salmonella Disease Research. Infection and Immunity, 2011. 79(5): p. 1806–1814. https://doi.org/10.1128/IAI.01369-10 PMID: 21343352

37. Mallett C.P., et al., Evaluation of Shigella vaccine safety and efficacy in an intranasally challenged mouse model. Vaccine, 1993. 11(2): p. 190–6. PMID: 8438617

38. Pepe J.C., et al., Pathogenesis of defined invasion mutants of Yersinia enterocolitica in a BALB/c mouse model of infection. Infect Immun, 1995. 63(12): p. 4837–48. PMID: 7591144

39. Heesemann J., Gaede K., and Autenrieth I.B., Experimental Yersinia enterocolitica infection in rodents: a model for human yersiniosis. APMIS, 1993. 101(6): p. 417–29. PMID: 8363822

40. Law R.J., et al., In vitro and in vivo model systems for studying enteropathogenic Escherichia coli infections. Cold Spring Harb Perspect Med, 2013. 3(3): p. a009977. https://doi.org/10.1101/cshperspect.a009977 PMID: 23457294

41. Reid B., Nuccitelli R., and Zhao M., Non-invasive measurement of bioelectric currents with a vibrating probe. Nat Protoc, 2007. 2(3): p. 661–9. https://doi.org/10.1038/nprot.2007.91 PMID: 17406628

42. Sun Y.H., et al., Airway Epithelial Wounds in Rhesus Monkey Generate Ionic Currents That Guide Cell Migration to Promote Healing. J Appl Physiol, 2011.

43. Reid B., et al., Wound healing in rat cornea: the role of electric currents. FASEB J, 2005. 19(3): p. 379–86. https://doi.org/10.1096/fj.04-2325com PMID: 15746181

44. Reid B., Song B., and Zhao M., Electric currents in Xenopus tadpole tail regeneration. Developmental Biology, 2009. 335(1): p. 198–207. https://doi.org/10.1016/j.ydbio.2009.08.028 PMID: 19733557

45. Clarke L.L., A guide to Ussing chamber studies of mouse intestine. Am J Physiol Gastrointest Liver Physiol, 2009. 296(6): p. G1151–66. https://doi.org/10.1152/ajpgi.90649.2008 PMID: 19342508

46. Deutsch A., et al., An uncommon presentation of Salmonella. Pediatr Emerg Care, 1996. 12(4): p. 285–7. PMID: 8858654

47. Tarnawski A. and Ivey K.J., Transmucosal potential-difference profile in rat upper gastrointestinal tract. A simple model for testing gastric effects of pharmacologic agents. Can J Physiol Pharmacol, 1978. 56(3): p. 471–3. PMID: 667721

48. Larsson M.H., et al., Elevated motility-related transmucosal potential difference in the upper small intestine in the irritable bowel syndrome. Neurogastroenterol Motil, 2007. 19(10): p. 812–20. https://doi.org/10.1111/j.1365-2982.2007.00941.x PMID: 17883433

49. Gustke R.F., et al., Human intestinal potential difference: recording method and biophysical implications. J Physiol, 1981. 321: p. 571–82. PMID: 6802960

50. Feil W., et al., Repair of rabbit duodenal mucosa after acid injury in vivo and in vitro. Gastroenterology, 1987. 92(6): p. 1973–86. PMID: 3569771

51. Okada Y., Irimajiri A., and Inouye A., Electrical properties and active solute transport in rat small intestine. II. Conductive properties of transepithelial routes. J Membr Biol, 1977. 31(3): p. 221–32. PMID: 845930

52. Okada Y., et al., Electrical properties and active solute transport in rat small intestine. I. Potential profile changes associated with sugar and amino acid transports. J Membr Biol, 1977. 31(3): p. 205–19. PMID: 845929

53. Wang J.Y., Yuan L.Z., and Wang M.D., [Effects of sodium artesunate on electrical properties and Na+, K(+)-ATPase activities of mouse small intestine]. Zhongguo Yao Li Xue Bao, 1990. 11(4): p. 335–7. PMID: 1966574

54. Amat C., et al., Electrical properties of the intestinal mucosa of the chicken and the effects of luminal glucose. Poultry Science, 1999. 78(8): p. 1126–1131. https://doi.org/10.1093/ps/78.8.1126 PMID: 10472838

55. Sundell K.S. and Sundh H., Intestinal fluid absorption in anadromous salmonids: importance of tight junctions and aquaporins. Front Physiol, 2012. 3: p. 388. https://doi.org/10.3389/fphys.2012.00388 PMID: 23060812

56. Adler J. and Shi W., Galvanotaxis in bacteria. Cold Spring Harb Symp Quant Biol, 1988. 53 Pt 1: p. 23–5.

57. Gebert A., et al., The development of M cells in Peyer's patches is restricted to specialized dome-associated crypts. American Journal of Pathology, 1999. 154(5): p. 1573–1582. https://doi.org/10.1016/S0002-9440(10)65410-7 PMID: 10329609

58. Buch E., et al., Transmucosal potential difference in experimental colitis in rats. Inflammation, 1995. 19(4): p. 445–55. PMID: 7558249

59. Zhao M., Electrical fields in wound healing-An overriding signal that directs cell migration. Semin Cell Dev Biol, 2009. 20(6): p. 674–82. https://doi.org/10.1016/j.semcdb.2008.12.009 PMID: 19146969

60. Santos R.L., et al., Life in the inflamed intestine, Salmonella style. Trends Microbiol, 2009. 17(11): p. 498–506. https://doi.org/10.1016/j.tim.2009.08.008 PMID: 19819699

61. Winter S.E., et al., Gut inflammation provides a respiratory electron acceptor for Salmonella. Nature, 2010. 467(7314): p. 426–9. https://doi.org/10.1038/nature09415 PMID: 20864996

62. Sawyer P.N. and Pate J.W., Electrical potential differences across the normal aorta and aortic grafts of dogs. Am J Physiol, 1953. 175(1): p. 113–7. https://doi.org/10.1152/ajplegacy.1953.175.1.113 PMID: 13114362

63. Sawyer P.N., Pate J.W., and Weldon C.S., Relations of abnormal and injury electric potential differences to intravascular thrombosis. Am J Physiol, 1953. 175(1): p. 108–12. https://doi.org/10.1152/ajplegacy.1953.175.1.108 PMID: 13114361

64. Sawyer P.N., Suckling E.E., and Wesolowski S.A., Effect of small electric currents on intravascular thrombosis in the visualized rat mesentery. Am J Physiol, 1960. 198: p. 1006–10. https://doi.org/10.1152/ajplegacy.1960.198.5.1006 PMID: 14442116

65. Sawyer P.N. and Wesolowski S.A., The electric current of injured tissue and vascular occlusion. Ann Surg, 1961. 153: p. 34–42. PMID: 13746959

66. Kaufmann S.H. and Schaible U.E., Antigen presentation and recognition in bacterial infections. Curr Opin Immunol, 2005. 17(1): p. 79–87. https://doi.org/10.1016/j.coi.2004.12.004 PMID: 15653315

67. Wang C., et al., Characterization of murine macrophages from bone marrow, spleen and peritoneum. BMC Immunol, 2013. 14: p. 6. https://doi.org/10.1186/1471-2172-14-6 PMID: 23384230

68. Valdez Y., Ferreira R.B., and Finlay B.B., Molecular mechanisms of Salmonella virulence and host resistance. Curr Top Microbiol Immunol, 2009. 337: p. 93–127. https://doi.org/10.1007/978-3-642-01846-6_4 PMID: 19812981

69. Baumler A.J., et al., Synergistic effect of mutations in invA and lpfC on the ability of Salmonella typhimurium to cause murine typhoid. Infect Immun, 1997. 65(6): p. 2254–9. PMID: 9169760

70. Finkelstein E.I., et al., Electric field-induced polarization of charged cell surface proteins does not determine the direction of galvanotaxis. Cell Motil Cytoskeleton, 2007. 64(11): p. 833–46. https://doi.org/10.1002/cm.20227 PMID: 17685443

71. McLaughlin S. and Poo M.M., The role of electro-osmosis in the electric-field-induced movement of charged macromolecules on the surfaces of cells. Biophys J, 1981. 34(1): p. 85–93. https://doi.org/10.1016/S0006-3495(81)84838-2 PMID: 6894257

72. Silva Filho F.C., et al., Surface charge of resident, elicited, and activated mouse peritoneal macrophages. J Leukoc Biol, 1987. 41(2): p. 143–9. PMID: 3468193

73. Park D., et al., Salmonella Typhimurium Enzymatically Landscapes the Host Intestinal Epithelial Cell (IEC) Surface Glycome to Increase Invasion. Mol Cell Proteomics, 2016. 15(12): p. 3653–3664. https://doi.org/10.1074/mcp.M116.063206 PMID: 27754876

74. Liu C.K., Wei G., and Atwood W.J., Infection of glial cells by the human polyomavirus JC is mediated by an N-linked glycoprotein containing terminal alpha(2–6)-linked sialic acids. J Virol, 1998. 72(6): p. 4643–9. PMID: 9573227

75. Foster J.W., Acid stress responses of Salmonella and E-coli: Survival mechanisms, regulation, and implications for pathogenesis. Journal of Microbiology, 2001. 39(2): p. 89–94.

76. Foster J.W. and Hall H.K., Adaptive acidification tolerance response of Salmonella typhimurium. J Bacteriol, 1990. 172(2): p. 771–8. PMID: 2404956

77. Allam U.S., et al., Acidic pH induced STM1485 gene is essential for intracellular replication of Salmonella. Virulence, 2012. 3(2): p. 122–135. https://doi.org/10.4161/viru.19029 PMID: 22460643

78. Beuzon C.R., et al., pH-dependent secretion of SseB, a product of the SPI-2 type III secretion system of Salmonella typhimurium. Mol Microbiol, 1999. 33(4): p. 806–16. PMID: 10447889

79. Chakraborty S., Mizusaki H., and Kenney L.J., A FRET-based DNA biosensor tracks OmpR-dependent acidification of Salmonella during macrophage infection. PLoS Biol, 2015. 13(4): p. e1002116. https://doi.org/10.1371/journal.pbio.1002116 PMID: 25875623

80. Cohen D.J., Nelson W.J., and Maharbiz M.M., Galvanotactic control of collective cell migration in epithelial monolayers. Nat Mater, 2014. 13(4): p. 409–17. https://doi.org/10.1038/nmat3891 PMID: 24608142

81. Sun Y., et al., Keratocyte fragments and cells utilize competing pathways to move in opposite directions in an electric field. Curr Biol, 2013. 23(7): p. 569–74. https://doi.org/10.1016/j.cub.2013.02.026 PMID: 23541726

82. McLaughlin L.M., et al., The Salmonella SPI2 effector SseI mediates long-term systemic infection by modulating host cell migration. PLoS Pathog, 2009. 5(11): p. e1000671. https://doi.org/10.1371/journal.ppat.1000671 PMID: 19956712

83. Figueira R. and Holden D.W., Functions of the Salmonella pathogenicity island 2 (SPI-2) type III secretion system effectors. Microbiology, 2012. 158(Pt 5): p. 1147–61. https://doi.org/10.1099/mic.0.058115-0 PMID: 22422755

84. Lombard V., et al., The carbohydrate-active enzymes database (CAZy) in 2013. Nucleic Acids Res, 2014. 42(Database issue): p. D490–5. https://doi.org/10.1093/nar/gkt1178 PMID: 24270786

85. Arabyan N., et al., Salmonella Degrades the Host Glycocalyx Leading to Altered Infection and Glycan Remodeling. Sci Rep, 2016. 6: p. 29525. https://doi.org/10.1038/srep29525 PMID: 27389966

86. Weber A.N., Morse M.A., and Gay N.J., Four N-linked glycosylation sites in human toll-like receptor 2 cooperate to direct efficient biosynthesis and secretion. J Biol Chem, 2004. 279(33): p. 34589–94. https://doi.org/10.1074/jbc.M403830200 PMID: 15173186

87. da Silva Correia J. and Ulevitch R.J., MD-2 and TLR4 N-linked glycosylations are important for a functional lipopolysaccharide receptor. J Biol Chem, 2002. 277(3): p. 1845–54. https://doi.org/10.1074/jbc.M109910200 PMID: 11706042

88. Crump J.A., et al., Part I. Analysis of data gaps pertaining to Salmonella enterica serotype Typhi infections in low and medium human development index countries, 1984–2005. Epidemiol Infect, 2008. 136(4): p. 436–48. https://doi.org/10.1017/S0950268807009338 PMID: 17686194

89. Erickson C.A. and Nuccitelli R., Embryonic fibroblast motility and orientation can be influenced by physiological electric fields. J Cell Biol, 1984. 98(1): p. 296–307. PMID: 6707093

90. Wu L., et al., The G protein beta subunit is essential for multiple responses to chemoattractants in Dictyostelium. J Cell Biol, 1995. 129(6): p. 1667–75. PMID: 7790362

91. Zhao M., et al., Genetic analysis of the role of G protein-coupled receptor signaling in electrotaxis. J Cell Biol, 2002. 157(6): p. 921–7. https://doi.org/10.1083/jcb.200112070 PMID: 12045182

92. Gao R.C., et al., A large-scale screen reveals genes that mediate electrotaxis in Dictyostelium discoideum. Science Signaling, 2015. 8(378).

93. Gordon S.V. and Parish T., Microbe Profile: Mycobacterium tuberculosis: Humanity's deadly microbial foe. Microbiology, 2018. 164(4): p. 437–439. https://doi.org/10.1099/mic.0.000601 PMID: 29465344

94. Luxardi G., et al., Single cell wound generates electric current circuit and cell membrane potential variations that requires calcium influx. Integr Biol (Camb), 2014.

95. Knodler L.A., et al., Dissemination of invasive Salmonella via bacterial-induced extrusion of mucosal epithelia. Proc Natl Acad Sci U S A, 2010. 107(41): p. 17733–8. https://doi.org/10.1073/pnas.1006098107 PMID: 20876119

96. Knodler L.A., et al., Noncanonical inflammasome activation of caspase-4/caspase-11 mediates epithelial defenses against enteric bacterial pathogens. Cell Host Microbe, 2014. 16(2): p. 249–56. https://doi.org/10.1016/j.chom.2014.07.002 PMID: 25121752

97. Celli J., Salcedo S.P., and Gorvel J.P., Brucella coopts the small GTPase Sar1 for intracellular replication. Proc Natl Acad Sci U S A, 2005. 102(5): p. 1673–8. https://doi.org/10.1073/pnas.0406873102 PMID: 15632218

98. de Jong M.F., et al., Identification of VceA and VceC, two members of the VjbR regulon that are translocated into macrophages by the Brucella type IV secretion system. Mol Microbiol, 2008. 70(6): p. 1378–96. https://doi.org/10.1111/j.1365-2958.2008.06487.x PMID: 19019140

99. O'Brien A.D., Rosenstreich D.L., and Taylor B.A., Control of natural resistance to Salmonella typhimurium and Leishmania donovani in mice by closely linked but distinct genetic loci. Nature, 1980. 287 (5781): p. 440–2. PMID: 7001248

100. Okoro C.K., et al., Signatures of adaptation in human invasive Salmonella Typhimurium ST313 populations from sub-Saharan Africa. PLoS Negl Trop Dis, 2015. 9(3): p. e0003611. https://doi.org/10.1371/journal.pntd.0003611 PMID: 25803844

101. Carden S.E., et al., Pseudogenization of the Secreted Effector Gene sseI Confers Rapid Systemic Dissemination of S. Typhimurium ST313 within Migratory Dendritic Cells. Cell Host Microbe, 2017. 21(2): p. 182–194. https://doi.org/10.1016/j.chom.2017.01.009 PMID: 28182950

102. Worley M.J., et al., Salmonella typhimurium disseminates within its host by manipulating the motility of infected cells. Proc Natl Acad Sci U S A, 2006. 103(47): p. 17915–20. https://doi.org/10.1073/pnas.0604054103 PMID: 17095609

103. Zhang X., Goncalves R., and Mosser D.M., The isolation and characterization of murine macrophages. Curr Protoc Immunol, 2008. Chapter 14: p. Unit 14 1.

104. Sun Y.H., et al., virB-Mediated survival of Brucella abortus in mice and macrophages is independent of a functional inducible nitric oxide synthase or NADPH oxidase in macrophages. Infect Immun, 2002. 70(9): p. 4826–32. https://doi.org/10.1128/IAI.70.9.4826-4832.2002 PMID: 12183526

105. Nakajima K., et al., KCNJ15/Kir4.2 couples with polyamines to sense weak extracellular electric fields in galvanotaxis. Nat Commun, 2015. 6: p. 8532. https://doi.org/10.1038/ncomms9532 PMID: 26449415

106. Zhao M., et al., Orientation and directed migration of cultured corneal epithelial cells in small electric fields are serum dependent. J Cell Sci, 1996. 109 (Pt 6): p. 1405–14.

107. Song B., et al., Application of direct current electric fields to cells and tissues in vitro and modulation of wound electric field in vivo. Nat Protoc, 2007. 2(6): p. 1479–89. https://doi.org/10.1038/nprot.2007.205 PMID: 17545984

108. Tai G., et al., Electrotaxis and wound healing: experimental methods to study electric fields as a directional signal for cell migration. Methods Mol Biol, 2009. 571: p. 77–97. https://doi.org/10.1007/978-1-60761-198-1_5 PMID: 19763960

109. Gruler H. and Nuccitelli R., Neural crest cell galvanotaxis: new data and a novel approach to the analysis of both galvanotaxis and chemotaxis. Cell Motil Cytoskeleton, 1991. 19(2): p. 121–33. https://doi.org/10.1002/cm.970190207 PMID: 1878979